Intraseasonal and synoptic modulation of diurnal surface solar radiation over Reunion island in the South-West Indian Ocean

Chao Tang [a,*], Pauline Mialhe [a], Benjamin Pohl [b], Béatrice Morel [a], Martin Wild [c], Shunya Koseki [d], Babatunde Abiodun [e], Miloud Bessafi [a], Chris Lennard [e], Girish Kumar Beeharry [f], Roddy Lollchund [f], Tyagaraja S.M. Cunden [g], Swati Singh [a]

[a] ENERGY-Lab, University of Reunion, 15 avenue René Cassin, CS 92003, 97744 Saint-Denis Cedex 9, Reunion, France
[b] Centre de Recherches de Climatologie, UMR6282 Biogéosciences, CNRS/Université de Bourgogne Franche-Comté, 6 boulevard Gabriel, 21000 Dijon, France
[c] Institute for Atmospheric and Climate Science, ETH Zurich, Universitätsstr. 16, 8092 Zurich, Switzerland
[d] Geophysical Institute, University of Bergen, Bjerknes Centre for Climate Research, Bergen, Norway
[e] Climate System Analysis Group, Department of Environmental and Geographical Sciences, University of Cape Town, Cape Town, South Africa
[f] Department of Physics, Faculty of Science, University of Mauritius, Mauritius
[g] Department of Electromechanical Engineering and Automation, Université des Mascareignes, Rose Hill, Mauritius

ARTICLE INFO

ABSTRACT

Understanding the space-time variability of Surface Solar Radiation (SSR) is mandatory for the prediction and, eventually, the skillful forecasting of photovoltaic energy production. This paper addresses the modulation of local-scale SSR over Reunion, a tropical island in the South-West Indian Ocean, by the leading modes of climate variability influencing both regional-scale and local-scale atmospheric convection and its associated cloud cover. Analyses focus on synoptic (tropical cyclones [TCs], synoptic convective regimes, including Tropical-Temperate Troughs [TTTs]) and intraseasonal (Madden-Julian Oscillation [MJO]) timescales. The SSR intra-daily variability is first assessed by a diurnal classification of SARAH-E satellite SSR data, and it is then related to the climate conditions mentioned above. SSR anomalies are found larger (smaller) on the windward (leeward) side of Reunion and in the summer (winter) season. The island-scale "cloudy" conditions can typically last 1 or 2 days. Nearby TCs can strongly reduce SSR by up to 50% on average, depending on their distances from Reunion, their sizes, and particularly, their longitudinal positions, which is observed for the first time. Nearby TCs are associated with significant negative SSR anomaly when located west of Reunion but with less significant or even positive anomaly when located east of the island. Synoptic convective regimes (the intraseasonal MJO) have a relatively weaker impact on SSR, with a value up to 13% (5%) of the mean value. Potential interactions between these SSR modulators are also investigated to understand better and eventually predict the mechanisms likely to modulate SSR (and thus photovoltaic electricity production) at sub-seasonal timescales.

1. Introduction

The impact of climate change has been observed worldwide in recent years, and it will continue to bring more frequent and more intense weather and climate extremes and stronger climate variability in the foreseeable future [1]. Mitigating and adapting to climate change are the most critical and difficult challenges of the 21st century. It is virtually certain that global surface temperature rise and associated changes can be limited through rapid and substantial reductions in Greenhouse Gas (GHG) emissions. About two-thirds of global GHG emissions are linked

to burning fossil fuels for energy to be used for heating, electricity, transport, and industry [2]. Therefore, energy transition to use clean, renewable resources is essential for moving towards a low-carbon future and mitigating climate change.

Solar energy is one of the most promising renewable and clean energy sources. The installation of solar photovoltaic (PV) electricity generation systems has continuously increased over the last decade. In 2020, over 135 GW of new solar PV were installed worldwide, increasing the total cumulative installed capacity to over 770 GW, and the 1 TW barrier was expected to be broken in 2022 [3]. The price of

solar electricity is decreasing rapidly [4], benefiting from the price reduction of solar panels and the associated battery storage to stabilize the electricity output.

In the South-West Indian Ocean (SWIO), where Reunion is located, many countries aim to increase the use of renewable and clean energy, notably solar power, to reduce their dependence on fossil fuels and decrease their GHG emissions [5,6]. For example, the Mauritius government has announced plans to increase the use of renewable sources for electricity generation to 60% by 2030. Solar energy will account for about 8% contribution to the electricity mix by 2020, while it was less than 1% in 2014 [7]. Reunion aims to achieve energy self-sufficiency based only on its renewable resources and become a "zero-net energy" island by 2030, with 27% from solar electricity [8,9]. In 2018, 36.5% of Reunion's electric production was from renewable energy sources, with 9% from PV systems [10]. However, the large variability of the local climate of Reunion still limits the integration of solar energy in the electric mix [11–13].

Solar energy is still facing a challenge regarding the uncertainty in electricity output, mainly due to the unpredictable, intermittent nature of Surface Solar Radiation (SSR). An accurate and complete assessment of SSR (mean state and spatiotemporal variability at different scales) is the basis of SSR forecasting [14–16]. This assessment is also necessary for the optimization of the electricity grid connected with multiple resources of renewable energy [17], such as solar-wind combination [18], and for the evaluation of the impacts of climate change on PV production [19,20]. The knowledge of the drivers of the space-time variability of SSR is, therefore, the starting point of its assessment.

A part of SSR variability is predictable and determined by the rotational and translational movements of the Earth with respect to the Sun. However, in addition to this, variability in SSR is also a function of the weather and climate systems. Like the climate system itself, SSR varies at different timescales: at the sub-daily scales mainly due to cloudiness and weather conditions, at the synoptic, intraseasonal to interannual scales due to climate variability, and at even longer timescales due to both low-frequency natural variability and human-introduced climate change (see for instance [21] for a review).

Reunion, located in the SWIO, experiences substantial SSR variability at different timescales [12,22–25]. Recently, the average annual and diurnal cycles of SSR and their spatial behavior over the island have been documented by Mialhe et al. [26] (M20 hereafter). However, SSR can also fluctuate spatiotemporally around its mean state due to either local effects at fine temporal and spatial scales or natural and/or anthropogenic climate variability at larger scales, which still need to be thoroughly investigated. This study focuses on the hourly/daily departures from these average SSR cycles. We then assess the role of convective variability from synoptic to intraseasonal timescales in shaping this SSR "anomaly".

At the synoptic timescale, Tropical Cyclones (TCs) in the SWIO develop mainly from December to March (referred to as DJFM hereafter; [27]). The associated strong convection can produce an abrupt reduction in atmospheric transparency and, thus, a significant attenuation of SSR. Even though TCs are rare events (~7% of days in DJFM have a nearby TC), their strong negative impact on SSR is essential to be characterized since these extremes are among the most severe and detrimental risks the island faces. As with other severe weather events [28], TCs could also challenge the survivability of solar farms.

Also at the synoptic timescale, regional convective regimes have been identified over the Southern Africa (SA)/SWIO region in the summer season from November to February (NDJF). It consists of seven robust and statistically well-separated patterns of large-scale organized convection, among which three regimes (regimes 5, 6, and 7, as shown in Supplementary Figure S1), indicative of well-defined tropical-temperate interactions, are known as synoptic-scale Tropical Temperate Troughs (TTTs, [29–35]). TTTs basically consist of short-lived (typically 3–7 days in NDJF), northwest-southeast-tilted large-scale convective cloud bands over SA and the SWIO. These moving convective systems,

which have been reported to have an impact on seasonal rainfall over SA (e.g., [32,36,37]) and Madagascar [38], are expected to impact the diurnal variability of SSR over Reunion during their lifecycles.

At the intraseasonal timescale, the Madden-Julian Oscillation (MJO, [39,40]) is the dominant mode of intraseasonal variability in the tropics (see also reviews by Madden and Julian [41], Zhang [42,43], and references therein). The MJO can be characterized as a coupled convective-wind tropical disturbance that develops in the tropical Indian Ocean and slowly propagates eastward to the Maritime Continent and then to the West Pacific basin with an intraseasonal cycle of 30–60 days [44,45]. MJO involves scale interactions across a broad spectrum, from the diurnal cycle to interannual variability [46]. Remarkably, the MJO has been linked with the intraseasonal variability of rainfall in East Africa [47,48], SA [36] and the SWIO [38,49]. However, the effects of the MJO on the diurnal variability of SSR over the SWIO are still unclear and need to be explored.

At lower frequencies, the year-to-year variability of SSR in Reunion could also partly be driven by the changes in global Sea Surface Temperature (SST) patterns at the interannual timescale, including El Niño/Southern Oscillation (ENSO), the Indian Ocean Dipole (IOD, [50,51]), and the Subtropical Indian Ocean Dipole (SIOD, [52]). Indeed, some significant correlations are found in the teleconnection maps (see Supplementary Figure S2) between the seasonal occurrence of the SSR anomaly classifications (see Fig. 2 and sections 2, 3) and the synchronous mean SST field. However, analyzing this lower-frequency climate variability as local SSR drivers requires longer time series, both reliable and homogeneous in time, and available at high spatial resolutions, that do not exist today for the SWIO.

Thus, this study aims to quantify the influence of sub-seasonal convective variability over the SWIO region on diurnal SSR variability in Reunion at high spatial resolution (~5 km). We focus on the dominant synoptic and intraseasonal timescales, which are responsible for the largest proportion of convective variance [53]. An effort is also made to quantify the degree of nonlinear interaction between these different timescales and their consequences on SSR variability in Reunion. This knowledge will improve our understanding of SSR variability and its links to climate variability and thus benefit long-lead predictions of SSR for the solar energy industry.

This paper is structured as follows: section 2 presents the climatology of SSR in Reunion, the data used in this study, and the methods employed to document SSR variability and to identify the convective climate variability. Section 3 is dedicated to the description of hourly departures from the averaged diurnal cycle of SSR, and then section 4 investigates its links with convective variabilities. The potential interactions between these SSR drivers are presented in section 5. Finally, the conclusion and discussion are made in section 6.

2. Context, data, and methods

2.1. Climate characteristics of SSR in Reunion

Reunion is a high volcanic island located in the SWIO. The average annual and diurnal cycles of SSR, which have been described in M20, are shaped mainly by (1) the location of the island in the SWIO, where trade winds are generally from the east in summer and from the southeast in winter [54]; and (2) its high altitude and complex topography (see Fig. 1) which makes the island an isolated and especially prominent obstacle to the atmospheric circulation in the SWIO. Hence, like most tropical islands with a marked topography, Reunion exhibits a strong contrast between its windward and leeward sides. According to M20, the averaged diurnal cycle depicts an east-west contrast with maximum values of SSR on the leeward side (at the west) of the island and minimum values on the windward side (at the east) in the early morning. This pattern then reverses over the day, leading to maximum values on the windward side and minimum values on the leeward side. This east-west difference in the mean diurnal cycle is related to the initiation and
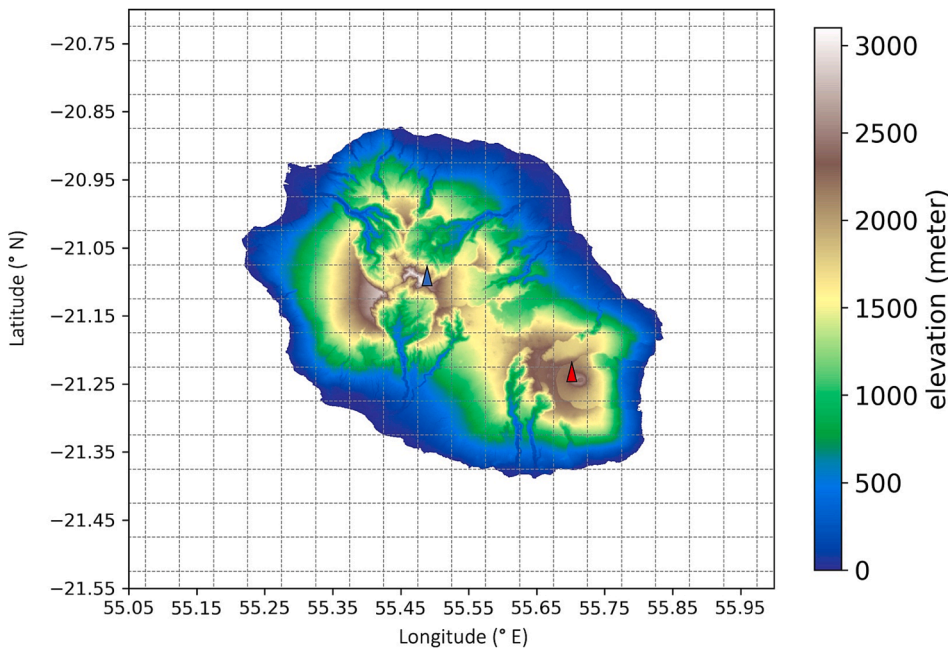
Fig. 1. Topography of Reunion (in meter) on SARAH-E grid (dotted gray lines). The 89 pixels over land are used for the diurnal SSR classification. This map is based on the ASTER Global Digital Elevation Model from NASA Jet Propulsion Laboratory [55]. The highest summits are depicted by triangles in color. The first one is the dormant Piton des Neiges volcano in blue, peaking at 3071 m asl (above sea level) in the center, and the other one is the active Piton de La Fournaise volcano, in red, at 2560 m asl in the east. Between these two lies a 1500 m-high plateau. Reunion exhibits a strong contrast between its windward (east) and leeward (west) sides, which is shaped by this remarkable topography and the seasonal changing trade wind direction, being from the east during the summer months (from November to April) and from the southeast during the winter months (from May to October). (For interpretation of the references to color in this figure legend, the reader is referred to the web version of this article.)

evolution of cloud cover on the island, which is driven by the development of orographic clouds due to the combined effects of trade winds and thermal winds on the windward side, and to thermal winds solely on the leeward side (M20). A similar east-west difference was found in rainfall, with overall higher amplitudes and variations in the island's windward side (at the east-southeast; [56]). The seasonality of this averaged SSR diurnal cycle is due to the annual changes in the synoptic wind direction and strength, and in the sea-land contrast. In addition, the island experiences extreme events such as heavy rainfalls and storms as well as TCs, whose effects on SSR can be enhanced by interacting with the marked topography [24,27,56–58]. Moreover, the complexity of the topography also has a considerable influence on the development of energy production sites because of their accessibility and thus impacts the energy storage/transferring strategy over the island.

2.2. SARAH-E SSR and diurnal SSR classification

The SSR data is taken from the regional climate data record of Solar surfAce RAdiation Heliosat - East (SARAH-E, [59,60]), which is derived from the observations onboard the geostationary METEOSAT Indian Ocean Data Coverage (i.e., IODC) satellites. Hourly instantaneous records are used throughout its entire period of availability, from 1999-01-01 to 2016-12-31 (YYYY-MM-DD; we exclusively use this time format thereafter, and hours are in REunion Time zone (RET) corresponding to GMT+4). During this period, only daytime records (from 8:00 to 17:00) of 6421 days are used for analysis, 154 days with missing records being removed. Spatially, 360 pixels cover the region of (55.05 to 56°E; −21.55 to −20.7°S), of which 89 pixels over Reunion are extracted at a spatial resolution of 0.05°, i.e., ~5.3 km at this location (Fig. 1).

The reliability of SARAH-E against in-situ measurements has been assessed over India [61], China [62], and particularly over Reunion by Bessafi et al. [12] and M20. The former showed that monthly means of SARAH-E estimates differ from the ground-based Météo-France SSR by approximately 10% on average, with higher errors locally. M20 reported differences of ~15% for diurnal-seasonal variations when compared with 32 Météo-France stations in Reunion over the period 2011–2015. SARAH-E is used in this study following M20, where the same was employed to represent the average annual and diurnal cycles of SSR over Reunion.

Firstly, hourly anomalies are calculated for each pixel by subtracting

the daily-hourly climatology. To obtain such a climatology, a 1st order low-pass filter (Butterworth filter with a cut-off frequency of 28 days) is applied to smooth out the high-frequency variations (values on the 29th of February are removed). The border effect has been treated by repeating the daily-hourly values in the entire 18 years three times so that the filter is applied on 54 values each day, each hour for each pixel, and only the filtered values in the center are taken as climatology for the following analysis. The calculation of the anomalies is expressed as the equation below:

$$SSR_{anomaly}(h, d, y) = SSR(h, d, y) - SSR_{climatology}(h, d)$$

where

$$SSR_{climatology}(h, d) = \frac{1}{n_{year}} \sum_{y=1999}^{2016} \left(SSR_{filtered(h, d, y)} \right)$$

and *h* stands for hour, *d* for Julian day, and *y* for year.

Then, a clustering approach is performed on these anomalies to assess SSR variability by regrouping the whole dataset (6421 daily-hourly SSR maps) into a small number of groups. The Ascending Hierarchical Clustering method is used here, where Ward's criterion [63] is applied to perform the successive groupings. The number of clusters finally retained is 9 by considering the clustering dendrogram (classification tree, see Supplementary Figure S3), the representativeness of characteristics of local temporal/spatial variability of SSR, and the abundance of details to be linked with larger scale climate variabilities in this study (see sections 3 and 4).

The resulting 9 clusters, shown by their mean profiles in Fig. 2, represent possible departures from the averaged diurnal SSR cycle. The synoptic transition behavior of these clusters (section 3), along with their distinct characteristics, such as the sign, amplitude, seasonality, and spatial pattern, enables the exploration and analysis of the underlying synoptic SSR variability.

The 1st cluster (i.e., CL1) shows a sign transition from predominantly positive to negative SSR anomalies around early afternoon; Similar sign transition could be observed in CL8 as well, with an earlier shift that occurs in the morning around 10:00. CL5 also presents a sign transition but from negative to positive.

There are also clusters with generally the same sign of anomaly throughout the day. For the positive ones: CL3 exhibits significantly larger values of SSR anomalies compared to CL4. Furthermore, CL3
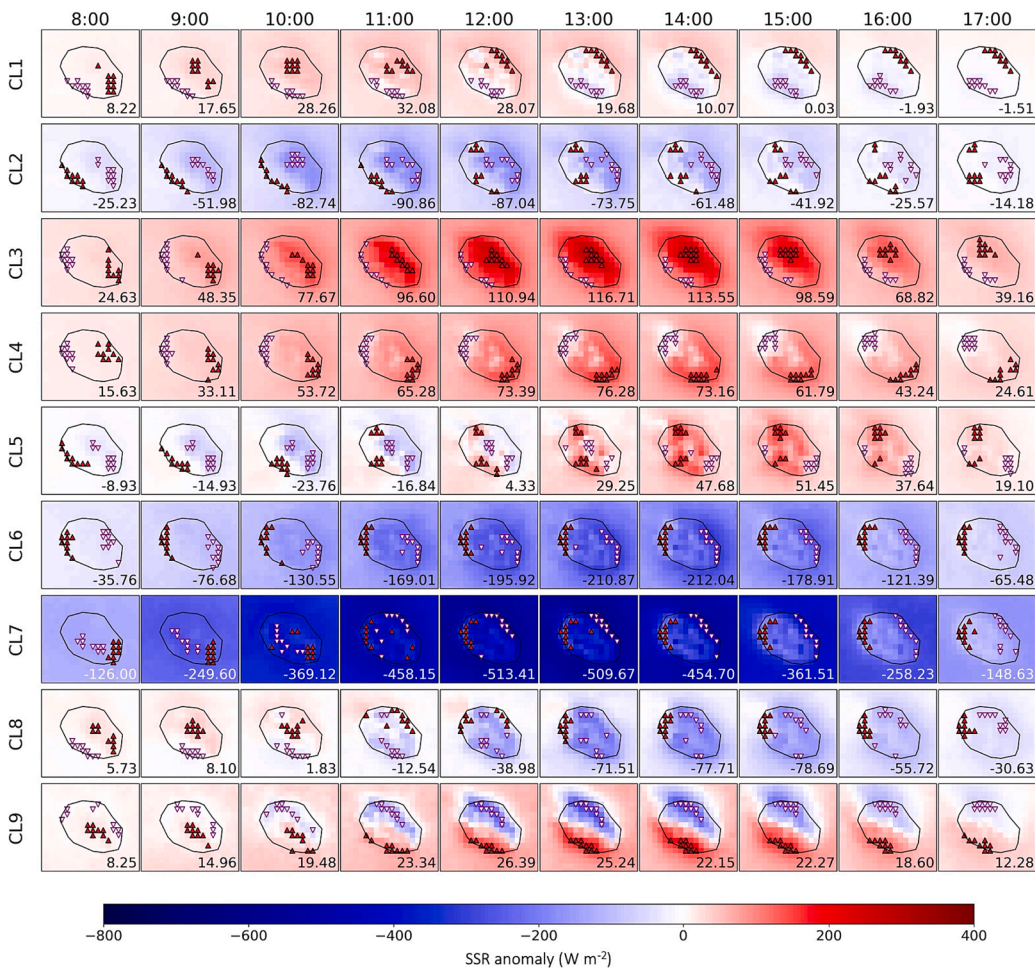
Fig. 2. Diurnal profiles of SSR anomaly over Reunion during the daytime hours from 8:00 to 17:00 local time for the nine clusters denoted as CL1–9. These clusters are obtained based on a hierarchical clustering of SARAH-E satellite data from 1999 through 2016 at 5 km spatial resolution over Reunion to assess the SSR intra-daily variability (see section 2.2 for a detailed description of the classification approach). Red up (purple down) triangles on each subplot locate the island pixels' 10 % maxima (minima) values. The mean values for each hour are displayed in the bottom right corner of the respective subplot (in black for all clusters except for cluster CL7, where it appears in white for clarity). The colorbar provides a visual representation of SSR anomaly values, measured in units of W m^{-2}, with positive anomalies depicted in red and negative ones in blue. The differences among these 9 SSR clusters are summarized in section 3 in terms of the amplitude, seasonality, spatial pattern, and cluster persistence and transition. (For interpretation of the references to color in this figure legend, the reader is referred to the web version of this article.)

demonstrates a more pronounced seasonal pattern, characterized by a higher frequency during the austral summer, whereas CL4 is present primarily during the austral winter. The spatial patterns are also different between these two clusters. Specifically, the maximum anomalies of CL3 tend to concentrate in the eastern and central regions of the island. In contrast, the most prominent anomalous pixels associated with CL4 are primarily located close to the southeast coast. This spatial divergence can be related to the distinct seasonality of the two clusters and the corresponding variations in the prevailing trade wind direction. For the negative clusters: CL2 maintains slightly negative anomalies from early morning to the end of the day, while CL6 and CL7 experience significant SSR attenuation. CL6 displays a maximum SSR attenuation of about 210 W m^{-2}, while the amplitude of CL7 is even higher, reaching up to 510 W m^{-2}. This notable reduction of SSR indicates a heavy cloudy sky condition, as usually observed in the case of a nearby TC.

Finally, CL9 exhibits a distinctive dipole pattern in SSR anomaly, which emerges around 10:00, with positive (negative) pixels observed in the southwest (northeast) region of the island. A dipole pattern, characterized by a north-south contrast, is also observed in CL1 (especially from 11:00 to 14:00). Nonetheless, it is noteworthy that CL1 exhibits a considerably weaker amplitude and an opposite sign compared to the dipole pattern observed in CL9.

These 9 clusters will be further investigated in section 3 to characterize better SSR variability. Subsequently, they will be linked to the intraseasonal convective variabilities as shown in section 4, including TCs, synoptic convective regimes (TTTs), and the MJO, aiming to explore the diurnal/local response of SSR in Reunion to the larger scale convective variabilities in the SWIO.

2.3. Best-track dataset of TC

TCs are characterized using the best-track data produced by the Regional Specialized Meteorological Center of Reunion from 1999 to April 2016 [27]. This data has cyclone records every 6 hours. Only the timestamps, cyclone positions, and the Radii of maximum wind speed (Rmax) are used in this study. The nearby cyclones are selected if within a distance of 5° from Reunion (21.1°S, 55.5°E) to take into account the possible impact considering the size of cyclone systems (the radius of the outermost closed isobar of a nonmidget event is about 400 km on the mean: [27]). A TC day is defined as having at least one of the 6-hourly records within that day.

2.4. ERA5 reanalysis and OLR regimes classification

Atmospheric fields used in this study are taken from the ERA5 ensemble reanalysis [64]. ERA5 is the fifth generation atmospheric reanalysis released by the European Centre for Medium-Range Weather Forecasts, providing either a deterministic member at a 0.25° × 0.25° global resolution or a 10-member ensemble available at a 0.5° × 0.5° resolution. We consider data from 1979 onward (the quality of the extension to 1940–1978 needs to be carefully assessed since the density, quality, and quantity of assimilated data are much lower in the absence of satellite data). Available variables consist of hourly gridded outputs of surface and atmospheric fields at the global scale. In this study, the top net thermal radiation (J m^{-2}, converted in W m^{-2}), corresponding to the net longwave radiation at the top of the atmosphere, is used to approximate large-scale atmospheric convection, an equivalent to the satellite-based Outgoing Longwave Radiation (OLR) used in previous

studies (e.g., [29], F09 hereafter; [31,32,35]). For convenience, this reanalysis-based field is referred to as OLR in the remainder of this study.

To obtain a set of recurrent synoptic-scale convective regimes for assessing the large-scale organization of atmospheric convection over SA, we replicate here the methodology proposed by F09 on ERA5 OLR. The method consists in a K-means clustering [65,66] of daily OLR anomalies in NDJF during 1979–2018, after removing its mean annual cycle. This has already been successfully used to deconstruct the ENSO influence over SA (F09), document the TTT life cycle [31,35], and assess its influence on rainfall over Madagascar and the nearby Mascarene Islands [38]. This method is applied to the unperturbed member of ERA5 ensemble at a $0.25° \times 0.25°$ resolution. Following F09, we define a partition into 7 clusters, these resulting clusters being both statistically significant (according to a so-called red-noise test: [66]) and physically coherent (F09). The 7 clusters (or regimes) are then projected onto the 10-member ensemble at an upscaled $0.5° \times 0.5°$ resolution following the methodology presented in Pohl et al. [32,67,68]. Member convergence and dominant cluster of the K-means clustering are shown in Supplementary Figure S4.

Among these 7 regimes, three (regimes 5, 6, and 7) correspond to the so-called TTT systems, differing primarily in their longitudinal location between SA (regime 5), the Mozambique Channel and Madagascar (regime 6), and the SWIO (regime 7, see Supplementary Figure S1). Regimes 3 and 4 are generally associated with sustained tropical convection (as denoted by negative OLR anomalies), with regime 3 interpreted as a potential precursor leading to regimes 4 and 5 (F09). In contrast, regimes 1 and 2 refer to the drier conditions over SA and materialize the decaying phases of the life cycle of TTT events, when the latter propagate further east towards the central Indian Ocean basin. For all regimes, OLR anomalies tend to be of larger magnitude than in F09, possibly due to a higher time sampling of the diurnal cycle of atmospheric convection in ERA5 and/or a much-increased spatial resolution ($0.25°$ for the unperturbed member and $0.5°$ for the 10-member ensemble in this study, vs. $2.5°$ for NOAA's satellite estimates used in F09).

2.5. MJO index

The Real-time Multivariate MJO (RMM) index of Wheeler and Hendon [45] used here is available from the 1st of June 1974 to present. The RMM index is derived from an Empirical Orthogonal Function (EOF) analysis of daily anomalies in upper- and lower-level zonal wind and OLR. MJO phases are defined by the principal components of the first two normalized leading EOFs (RMM1 and RMM2). The dominant eastward propagation of the MJO along the equator is described by 8 different phases in the two-dimensional RMM1 and RMM2 index phase space, and the amplitude of the MJO signal is provided by the distance from the origin. A large distance indicates a strong cycle of the MJO, while a small distance denotes weak activity when the MJO is not discernible above the atmospheric noise. In this study, the significant MJO events with amplitude >1 in NDJF over the period of SARAH-E (1999 – 2016) are used to have prominent results.

OLR anomalies of the 8 MJO phases in NDJF with high amplitude (>1) over the SWIO are shown in Supplementary Figure S5. For reference, during phase 1 of the MJO, weak convection exists over tropical Africa and the tropical Indian Ocean. During phases 2–4, this convection strengthens over the Indian Ocean and moves eastward, reaching peak intensity during phases 4 and 5 over the Maritime Continent. As the core MJO convective cluster moves into the Pacific Ocean, convection is suppressed across the Indian Ocean and over tropical Africa during phases 5 and 6, propagating towards the Maritime continent where strong suppression occurs in phases 7 and 8. The SSR anomaly is expected to be altered according to the propagation of the enhanced/suppressed convection close to Reunion.

3. SSR diurnal variability in Reunion

The average annual and diurnal cycles of SSR in Reunion are modulated by large-scale climate conditions that drive major changes in cloud formation. These diurnal profiles of hourly SSR anomalies (calculated against a smoothed daily-hourly climatology) are concisely characterized, at each pixel, by a classification (see section 2.2 for more details). The resulting clusters are further discussed below in terms of seasonality, spatial pattern, and cluster persistence and transition.

3.1. Diurnal SSR anomaly profile

The 9 clusters of diurnal SSR anomaly profiles are shown in Fig. 2. During the 1999–2016 period, ~55% of the total available days (6421 days) are assigned to groups whose anomaly patterns consist primarily of uniform-sign departures from the mean, for each pixel over and near the island and for each hour of the corresponding days. These clusters are hereafter referred to as uniform-sign clusters: they indicate a high probability (more than half of the total days) of constant-sign SSR changes from the mean state throughout the day at the scale of the island. In these clusters, ~34% of the days are associated with positive anomalies (CL3, 4) and ~21% with negative anomalies (CL2, 6, 7). In contrast, the remaining days ascribed to CL1, 5, 8, and 9, which represent slightly less than half of the days (~45%), are associated with differential spatial/diurnal changes in the signs of anomaly over the island. These clusters characterized by mixed-sign pixels are referred to as mixed-sign clusters hereafter. For these clusters, positive anomalies are generally found in CL1 before 11:00, while negative anomalies start to increase and become dominant over land after 14:00. CL8 shows a similar behavior with anomalies changing from positive to negative during the day, but the transition occurs earlier in the morning (around 10:00–11:00). Symmetrically, CL5 depicts a change from negative to positive anomalies during the day. CL9 presents a dipole pattern of SSR anomaly from 10:00 to the end of the day, with positive (negative) pixels in the southwest (northeast) of the island. These first results lead us to draw a first conclusion for solar energy production: deploying solar panels over the most contrasted and most complementary sites of the island could increase the efficiency of such a distributed network only about half of the time.

3.2. Seasonality

The 9 SSR clusters are not evenly distributed in each season (Fig. 3). CL1 (CL3) shows strong seasonality, with higher frequency in austral winter (summer) months. In general, the clusters with the largest anomalous SSR, either positive (CL3) or negative (CL7), are likely to be found in the warm season. By contrast, the uniform-sign clusters with less pronounced anomalies (the positive CL4 and the negative CL6) primarily occur in the cold season. The annual and diurnal modifications of each of the 9 SSR anomaly profiles are shown in Fig. 4, which again depicts a similar seasonality of the amplitude of the diurnal SSR patterns inside each cluster as an overview of the orbital variability of SSR.

3.3. Spatial pattern

Between the windward and the leeward sides of Reunion, major differences in rainfall [56] and SSR (M20) have been previously reported. Similar differences are also observed in diurnal SSR anomalies. As shown in Fig. 2, in the positive anomaly uniform-sign clusters (CL3, 4), an anomaly gradient, roughly oriented from the windward to the leeward side, is found throughout the day. The 10% highest values of SSR anomaly on Reunion (depicted by the red up triangles) are mainly located on the windward side of the island, while the 10% lowest values (depicted by the white down triangles) are on the leeward side. This pattern remains overall the same regardless of the season: CL3 has a strong seasonality with higher occurrence in the warm season, while
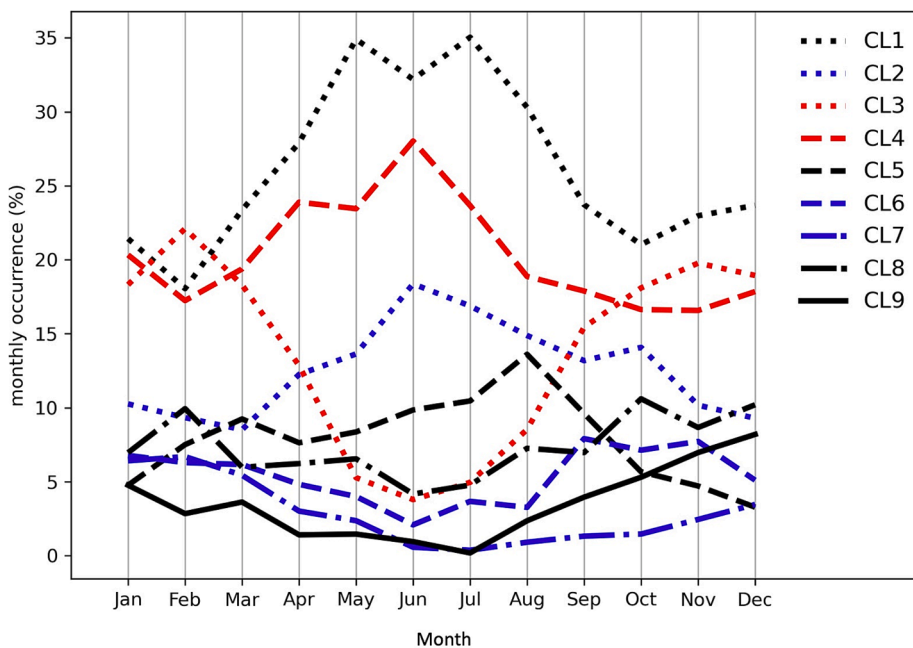
Fig. 3. Monthly occurrence (%) of the nine clusters of diurnal SSR anomaly (CL1–9, see Fig. 2) derived from the hierarchical clustering approach as described in section 2. Red lines indicate clusters with positive anomalies all over Reunion Island, including clusters 3 and 4 (i.e., CL3 and CL4). Blue lines, on the other hand, depict clusters with negative anomalies all over the island, including CL2, CL6, and CL7. The remaining clusters, i.e., CL1, CL8, and CL9, which exhibit a mixture of positive and negative anomalies over the island, are represented by black lines. These 9 SSR anomaly clusters are not evenly distributed in each season. However, the ones with higher amplitude, either positive (CL3) or negative (CL7), are found more frequently in summer (from Nov to Apr) than in winter (from May to Oct; see section 3.2 for further details). (For interpretation of the references to color in this figure legend, the reader is referred to the web version of this article.)

CL4, which depicts similar spatial patterns, has more occurrence in the cold season. This similarity of diurnal SSR anomaly patterns in the annual cycle can also be observed inside each cluster, as shown in Fig. 4. It is worth noting that in the cold season, when the island experiences a southerly anomaly of trade winds [56], the windward and the leeward zones are changed accordingly from east-west to southeast-northwest.

In contrast, in the negative anomaly uniform-sign clusters (CL2, 6), the anomaly patterns are generally reversed, with the pixels of the maximum anomalies on the leeward side and the minimum ones on the windward side, once again regardless of season (Fig. 4): CL2 is likely to be found more frequent in winter and CL6 in summer (Fig. 3). Additionally, the spatial patterns of the anomaly gradient, i.e., the windward-leeward difference, in most of the uniform-sign clusters, also remain the same throughout the day. This is especially the case for CL2, 3, 4, and 6 (except CL7), which occur in roughly 52% of the days of the studied period (Table 1). However, this windward-leeward difference is not evident in the mixed-sign clusters, whose spatial patterns vastly change during the day (Fig. 2). The SSR anomaly gradient, mainly observed in the uniform-sign clusters, implies a departure from the average diurnal SSR with higher amplitude on the windward than on the leeward side of Reunion.

3.4. Cluster persistence and transition

The mean persistence of each SSR anomaly cluster, expressed as a duration of day, is shown in Table 1 (last column; more details can be found in Supplementary Table S1 and Supplementary Figure S6). The overall short persistence, less than about 1.5 days, confirms that the transient disturbance of SSR, represented by the SSR clusters, is at the synoptic timescale. This quick succession suggests that successive days can have quite different SSR over the island and thus, different energy production. Technologies such as complementary and storage optimization are needed to smooth out the corresponding instability caused by these synoptic SSR disturbances.

Generally, the positive anomaly clusters (CL3 and 4) have higher persistence (>1.33 days) than the negative ones (CL2, 6, and 7, less than 1.29 days) since the less cloudy days are usually associated with more stable conditions. The persistence of the negative SSR group, consisting of all negative SSR clusters (i.e., CL2, 6, and 7), is quantified to better characterize SSR intermittency at synoptic timescale, as shown by a

violin plot in Supplementary Figure S7. It indicates the number of successive days that could have energy production below expectations, which is crucial for stabilizing the solar power output, such as dimensioning the storage facilities of PV systems. The majority of the successive negative events can last from 1 to 2 days (the 75th percentile), which again confirms the synoptic nature of SSR clusters. Efforts to stabilize solar power networks would be required to account for this intermittency.

With a large number of occurrences, the mixed-sign cluster CL1 has the highest probability (~35%) of persisting until the following day. By contrast, CL9 with a dipole pattern of SSR anomaly is the most unlikely to persist in the 9 clusters, with a value of about 1 day (see Supplementary Table S1). Then it is likely to be followed by the clusters with the highest occurrence, i.e., the positive-sign CL4 (26.8%) or the mixed-sign CL1 (20.9%).

The transition between SSR anomaly clusters, as shown in Table 1, can give insight into synoptic SSR changes. This table shows the total number of days in each SSR cluster (2nd column, followed by a ratio to the total available days) as well as the percentage of those days that are followed by days in the same and other clusters (inner part of the table, columns 4–12). These can be seen as the conditional probabilities of cluster transitions. The highest percentages observed on the diagonal of the inner part of the table give an indication of high probability of self-transition of each cluster. In contrast, CL2 is an expectation in which the most possible preceding cluster is CL7 (23.6%, comparable with the second highest possibility of 22.0% for self-transition) with high-amplitude negative SSR anomaly.

Continuity in the transition between uniform-sign clusters is evident: the positive/negative anomaly clusters have a probability of about 46.6/ 36.2% (not shown) to maintain their daily sign of SSR anomaly to the next day. However, the transition between positive and negative anomaly clusters has a much lower probability, with 14.4% for a transition from positive to negative on the next day and 21.8% for the inverse transition. Inversely, the transition from mixed-sign clusters to uniform-sign clusters is 30% for the positive anomaly clusters and 18.3% for the negative ones, which indicates a higher possibility of shifting from partly cloudy to an overall less cloudy condition at synoptic timescales over the island than the inverse.

A transition from CL7 (or CL6) to CL2 with a probability of 23.6% (or 15.5%) could be regarded as a synoptic brightening process at island-
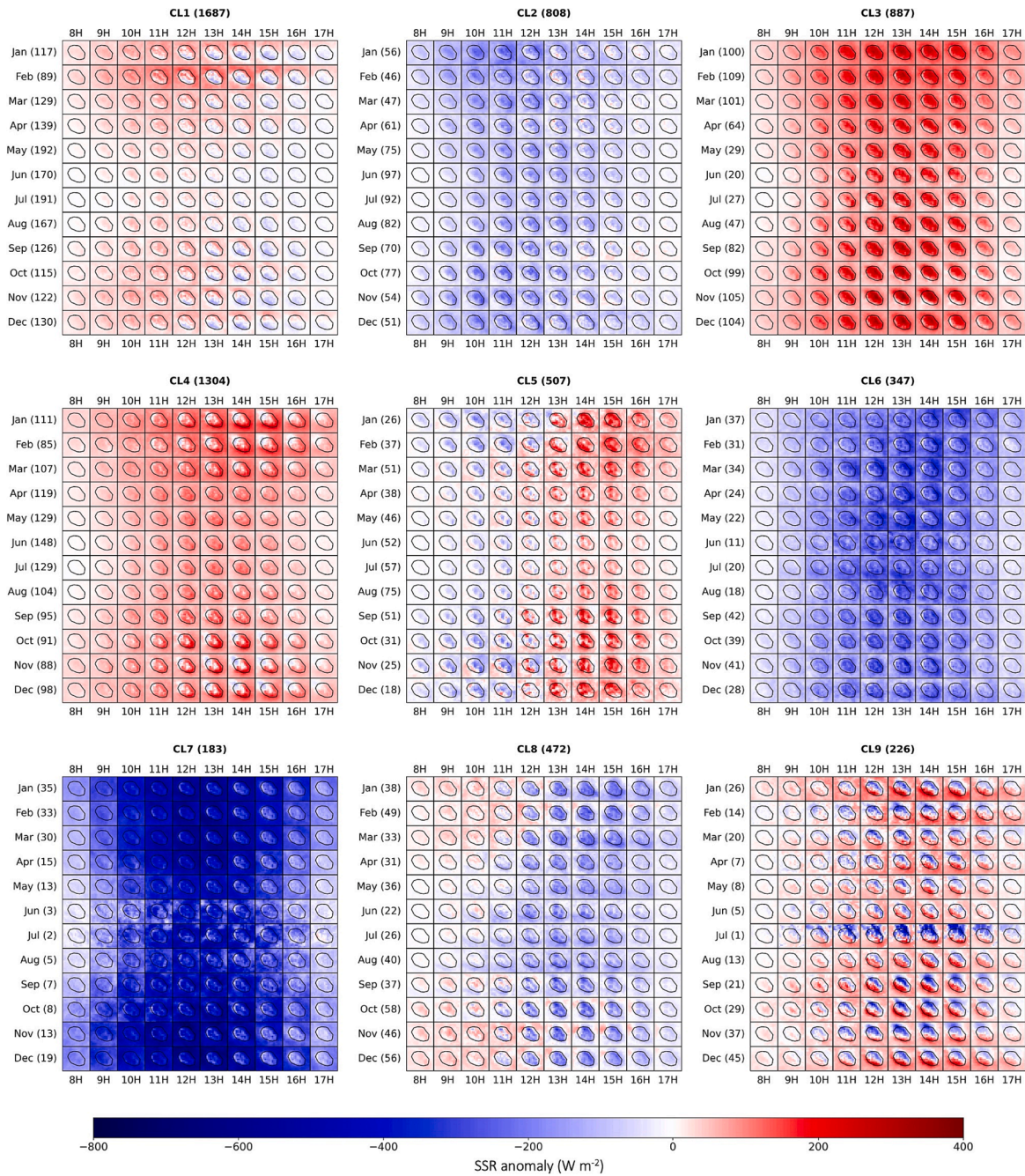
Fig. 4. Monthly mean diurnal SSR anomaly for the 9 SSR clusters (CL1–9, see Fig. 2) derived from the hierarchical clustering approach as described in section 2. The number of days in each month is shown in brackets with vertical labels. Values following cluster names are the total number of days in that cluster. This figure represents the orbital variation, i.e., annual and diurnal cycles of SSR in Reunion. The spatial patterns are quite similar within each cluster, which proves the reliability of the classification approach. More pronounced SSR anomalies are generally found in the summer months (November to April) than in the winter months (May–October). Further details are given in the text.

scale such as in the days with a nearby TC moving away from Reunion. Symmetrically, the island-scale synoptic dimming process depicted by the transition between the uniform-sign clusters, from CL2 to CL6 (or CL7), is much more unlikely to be observed, as the probability from CL2 to CL6 is 6.9% and that from CL2 to CL7 is 3.1%. The island-scale dimming from CL3 to CL4 is 19.5% and the brightening from CL4 to CL3 is 15%, which is comparable in both cases to the probability of transition between positive and negative anomaly clusters discussed above.

4. Modulation of SSR by convective variability

4.1. TC

A nearby TC can produce strong negative departures from the average diurnal cycle of local SSR, which can be seen in the SSR classification, such as in CL7 (Fig. 2). For this cluster, 50 days out of 183 (23.0%) have a nearby TC with a distance of less than 5° of Reunion (Supplementary Figure S8), which is much more than in the other negative SSR anomaly clusters (~4.3% in CL6; 3.3% in CL2) and the positive/mixed-sign ones (less than 3.1%). CL7 is characterized by

Table 1

Number and percentage of occurrences of each SSR cluster (columns 2, 3) and percentage of days followed by the same or another cluster (columns 4–12). The diurnal profiles of the SSR clusters are shown in Fig. 2. The mean persistence as the number of days is given in the last column. Red (blue) colors in the table headers depict the clusters with a uniform sign of positive (negative) SSR anomaly. Clusters with a mixed-sign in SSR anomaly are in gray in the table headers. Note that the number of day i + 1 is not always equal to the number of day i, since SARAH-E has missing data. More statistics of persistence can be found in Supplementary Table S1. (For interpretation of the references to color in this table, the reader is referred to the web version of this article.)

day = i			day = i + 1 (%)									mean persistence (day)
Cluster	day	%	CL1	CL2	CL3	CL4	CL5	CL6	CL7	CL8	CL9	
CL1	1687	26.3	35.3	9.4	11.1	19.4	5.6	5.4	2.0	8.8	3.0	1.43
CL2	808	12.6	22.0	22.0	9.8	15.4	11.8	6.9	3.1	6.0	3.1	1.28
CL3	887	13.8	21.0	9.0	26.6	19.5	9.2	3.8	2.8	5.4	2.7	1.33
CL4	1304	20.3	24.4	10.1	15.0	31.9	7.3	2.7	0.8	4.7	3.1	1.42
CL5	507	7.9	20.2	18.0	15.0	18.2	19.0	3.6	2.0	3.2	0.8	1.22
CL6	347	5.4	24.6	15.5	7.6	12.0	4.1	15.5	5.6	10.0	5.0	1.15
CL7	183	2.9	18.1	23.6	6.0	4.9	4.4	7.7	22.5	5.5	7.1	1.29
CL8	472	7.4	31.7	10.4	9.8	12.1	2.4	6.9	3.9	18.2	4.6	1.21
CL9	226	3.5	20.9	6.4	15.0	26.8	5.0	5.0	0.9	7.7	12.3	1.15

strong negative SSR anomalies (up to about −500 W m^{-2}) during the whole day, indicating strong and persistent cloud cover, such as in TC days. Additionally, this cluster also has the lowest occurrence (3%), in agreement with the relative rareness of TCs in this area (~2.5% of the days between 1999 and 2016 have nearby TCs). Moreover, CL7 has a strong seasonality with more occurrence in austral summer, which fits with the core of cyclone season in the SWIO (i.e., DJFM, which consists of nearly 94% nearby TC days in this season, also see [27]). The zonal anomaly gradient in CL7 changes from east-west to west-east during the day in contrast with the other negative uniform-sign clusters with a stable gradient all day. This change in the diurnal cycle of local SSR implies a drastic evolution of the atmospheric conditions, as the one observed in the case of a TC, as nearby cyclones can produce abrupt changes in the atmospheric circulation at island-scale within a day, especially when interacting with a complex topography like in Reunion [69]. Finally, the link between CL7 and TCs can also be found in the transition of the SSR anomaly clusters. CL7 has a higher probability (53.8%, not shown) to transmit to a negative uniform-sign cluster (CL2, 6, and 7) compared to CL2 (30.0%), CL6 (36.6%), and other clusters

(less than 22%). This transition from the most pronounced negative cluster, i.e., CL7, to other clusters with moderate attenuation (i.e., brightening) can happen during the passage of a nearby TC at synoptic timescale.

The diurnal response of local SSR to the nearby TCs through their strong attenuation can be quantified more precisely by comparing the mean diurnal cycle of SSR during TC days with non-TC days. In DJFM and during the study period (1999–2016), 152 days with TCs (10 TC days in other months) evolving near Reunion (i.e., within 5° of the island) are associated with a spatial mean hourly SSR of ~25% lower than during the 1988 non-TC days (see Supplementary Figure S9: if applying a smaller distance of 3°, instead of 5°, this value can increase to 50%, not shown). More precisely, TCs' influence on SSR strongly depends on their relative location with respect to the island and on their strength (shown as Rmax, in Fig. 5). First, the east-west difference is quite obvious, indicating that TCs in the west of Reunion are generally associated with negative SSR anomaly over the island. In contrast, TCs in the east are associated with less SSR attenuation or even positive SSR anomaly. The diurnal cycle of SSR anomalies during the eastern TC days shows very
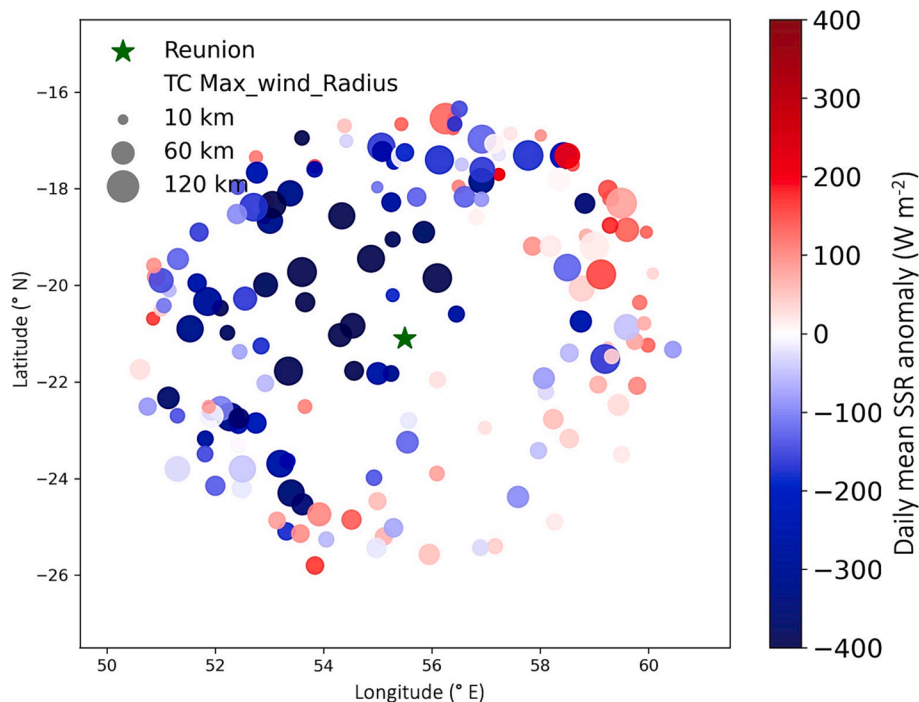

Fig. 5. Locations of TCs within 5° of Reunion (the green star) and the associated daily mean SSR anomalies over Reunion land area (colorbar). Symbol size depicts the Rmax (i.e., Radii of maximum wind speed in km) of each cyclone. (For interpretation of the references to color in this figure legend, the reader is referred to the web version of this article.)

few significant pixels over land, and much of them are positive (Supplementary Figure S10) located on the west coast with the steepest slopes of Reunion. In contrast, in the western TC days, SSR anomalies are generally negative throughout the day with a value from −90 to −260 W m^{-2} (much higher than that for the east TC days, that is, from –32 to 92 W m^{-2}), except for some pixels with non-significant results in the west coast of the island (Supplementary Figure S10). These geographical dependencies could be necessary for SSR predictability at the synoptic timescale, considering the typical lead time of cyclone track forecasting of about one week [70]. Second, a significant correlation between the TC size and their influence on SSR over Reunion is also found. The linear correlation between Rmax and the land-area SSR anomaly is −0.7 (−0.4) within 3 (5) degrees of Reunion. This is consistent with an earlier study that demonstrates a detectable orography impact of Reunion on TC track and intensity at less than 250 km from the island [69]. The mean passing time of all recorded nearby TCs, within 5° is from 1 to 6 days with an average value of about 2.7 days (Supplementary Figure S16), when local SSR could be potentially modulated by the strong evolution of the cloud condition associated with TCs.

4.2. Synoptic convective regimes

SSR variability over Reunion can also be potentially modulated by the synoptic convection regimes. Seven synoptic-scale convective regimes over SA and the SWIO based on OLR are identified by classification, where 3 of them are defined as TTTs (see Supplementary Figure S1 and section 2.4). The strong negative OLR anomalies in the OLR regimes are associated with the deep convection and thus coincide with a positive cloudiness/rainfall anomaly (F09). To investigate the synoptic modulation of local SSR variability over Reunion in these regimes, their association with SSR anomaly and contingency with SSR classification are examined (Fig. 6 and Fig. 7, respectively).

The diurnal cycles of SSR anomaly in the OLR regimes are shown in Fig. 6. Generally, the local SSR anomalies over Reunion and the surrounding ocean are overall consistent with the large-scale atmospheric

configurations associated with the OLR regimes in terms of their signs, amplitudes, and spatial patterns, although insignificant anomalies are found over land or even with some reverse sign signals.

The sign of SSR anomaly is strongly linked to the OLR regimes (Fig. 6). In OLR regimes 1 and 2, negative SSR anomalies are observed overall, which is consistent with the enhanced convective activities close to Reunion, in the northeastern of Madagascar and Reunion for regime 1, and centered in the SWIO, with extension from the southeastern part of Madagascar to around 30°S and 70°E for regime 2. Regimes 3, 5, and 6 are associated with overall positive SSR anomaly over Reunion and the surrounding ocean area (Fig. 6), again consistent with the sign of the OLR anomalies at large scale (Supplementary Figure S1). During regime 3 and the two first TTT regimes (i.e., regimes 5 and 6, corresponding to westernmost and central TTT locations), the area covering Reunion experiences suppressed convective conditions. Positive SSR anomaly is found in these regimes, with higher amplitude in regime 6 than in regimes 3 and 5, consistently with the highest positive OLR anomaly found locally for that regime. Such conditions of suppressed convection are caused by the mid-latitude wave pattern associated with TTTs, consisting of alternating positive, negative, and positive OLR anomalies from east to west (F09). In regime 7, where the TTTs reach their easternmost location, Reunion is located between the enhanced and suppressed convection bands, hence the lack of significant SSR anomaly in the island's surroundings. This association can also be found in the contingency map (Fig. 7). For example, regime 6 favors more positive SSR clusters (CL3 and CL4, though without statistical significance) and, at the same time, less negative SSR clusters (CL6, 7).

The amplitude and spatial extension of significant SSR anomalies are also in good agreement with the amplitude of the OLR anomalies covering Reunion. The SSR anomalies are of low amplitude and barely significant when the OLR anomaly is close to zero (e.g., regimes 4 and 7). Then an increase in the amplitude and an extension of the significant area are found in the regimes with higher OLR anomaly, either positive in regimes 3, 5, and 6 or negative in regimes 1 and 2.

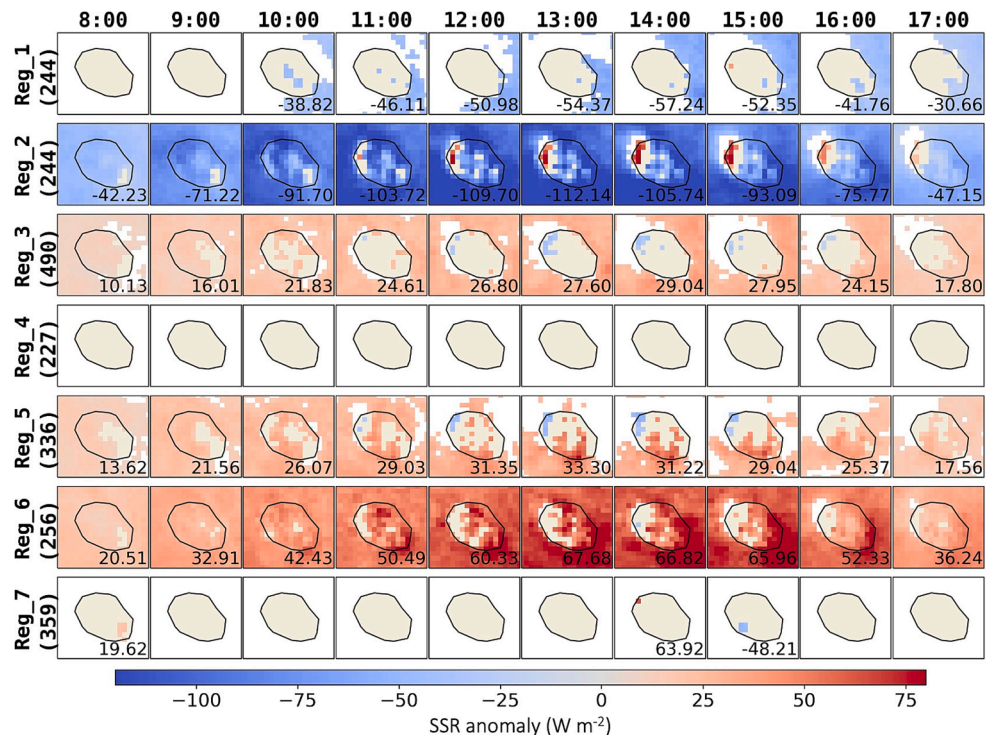Finally, the SSR anomalies display amplitudes that follow the diurnal

Fig. 6. SARAH-E SSR anomaly in seven OLR convective regimes in NDJF. Regimes 5–7 are associated with the so-called TTTs (section 2.4). Only pixels with significant SSR anomalies are presented in color according to Student's t-test with the False Discovery Rate (FDR; [71]) correction at the 0.05 confidence level. Values in the vertical axis indicate the number of days in each OLR regime.
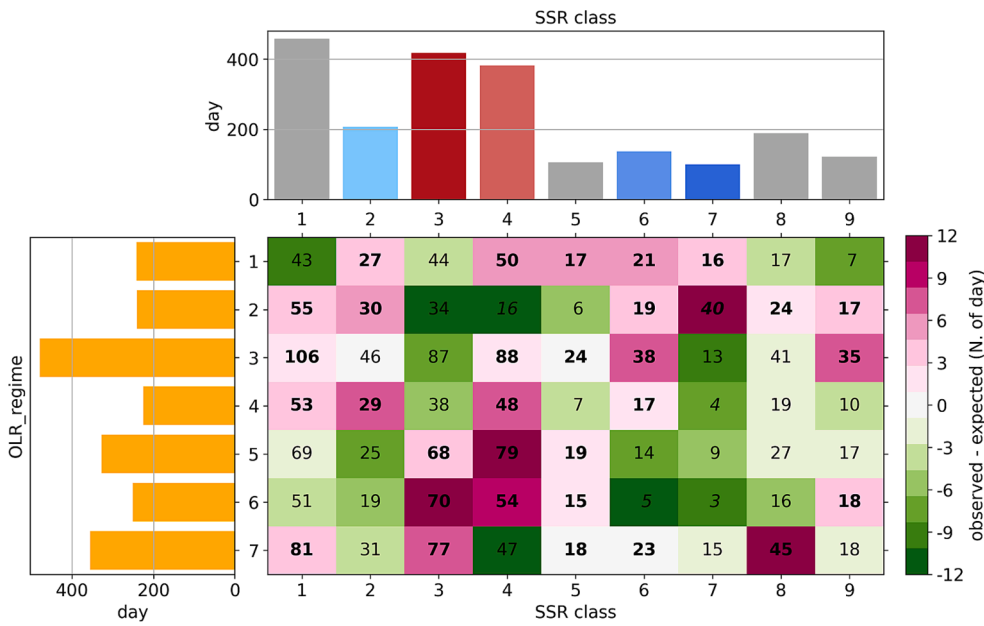
Fig. 7. Contingency map between SSR clusters (top bar plot) and synoptic convective regimes (left bar plot) in NDJF. In the top bar plot, red (blue) colors depict the clusters with a uniform-sign of positive (negative) SSR anomaly. Clusters with a mixed-sign in SSR anomaly are in gray. Values in the bottom right table are the occurrence in terms of the number of days of SSR clusters. Boldface values are overrepresented, and the other values are underrepresented. Italics denote 95% significance according to Neu's test. The difference in number of days between observed and expected days are presented by colors, with dark pink (green) for more (less) observed days than expected. (For interpretation of the references to color in this figure legend, the reader is referred to the web version of this article.)

cycle of SSR in almost all the OLR regimes, being smaller in the morning, then peaking at local solar noon and decreasing in the afternoon to sunset. The hourly SSR anomalies have a nearly constant ratio with the multiyear mean value in NDJF throughout the day (Supplementary Figure S11), ranging from 3% to 13% for different regimes.

However, some disagreement with the larger-scale variability is also found. Close to the western coast of the island, where the steepest slopes of Reunion are located, some pixels display a significant opposite sign to the overall SSR anomaly. In regime 2, associated with enhanced convection at a large scale, positive SSR anomalies are found after 11:00 local time. For regimes 3 and 5, in which clear-sky conditions prevail, negative SSR anomaly is observed from late morning onwards in the same location. Since such localized signals cannot be explained by large-scale convective activity, the role of local-scale effects associated with land-sea contrasts, such as the topography or surface properties (albedo, land-use, sea-land/mountain-valley breeze system, etc.) and short-term variability in monsoon flow, needs to be considered, which warrants further investigation using high-resolution regional climate modeling.

The strong attenuation of SSR in regime 2 (with a minimum value of about -112 W m^{-2} at around 13:00, which corresponds to more than 12% of the multiyear seasonal mean value) implies very high optical depth in the atmosphere, such as the case in heavy clouds associated with a TC. It is also evident in the contingency map (Fig. 7), where Neu's test [72] is applied to identify which single SSR cluster is significantly associated with synoptic regimes (occurring more or less frequently than the average). It is shown that regime 2 favors statistically significantly less positive SSR clusters, i.e., CL4, and at the same time significantly more negative SSR clusters, i.e., CL7. In addition, the occurrence of CL7 (linked to nearby TCs) within the OLR regime 2 (40 days) is extremely high, about 30 days more than expected when assuming independence of the SSR anomaly with the OLR regimes. However, regime 1 produces much less SSR anomaly (less than 60 W m^{-2}) than regime 2, which will be further investigated in section 5.1, where the interaction between TCs and OLR regimes is addressed.

4.3. MJO

SSR over Reunion can also be modulated by convective activities at larger timescales. The MJO at intraseasonal timescale is investigated in this section, even though it has a relatively more minor OLR variance compared with the synoptic convective regimes (about three times

smaller even at different timescales, see Macron et al. [38]), and it evolves in a much larger spatial extension, nearly global, with a convective center in the tropical band and thus within a distance to Reunion. The analysis is made in austral summer in NDJF since 1) the magnitude of SSR anomaly is larger in this warm season (section 3.2); and 2) the MJO activity itself shows seasonal meridional migrations that follow convection and the Inter Tropical Convergence Zone (or ITCZ), which are stronger in this season at the latitude of Reunion ($-21.55°$S; see, e.g., [45,73]). The 8 phases of the MJO (with amplitude > 1) in NDJF are then selected (see Supplementary Figure S5). The MJO modulation of SSR is investigated by computing the average SSR anomaly over Reunion in these 8 MJO phases (Fig. 8) and by assessing the contingency with the diurnal SSR classification (Fig. 9).

Composites of intra-daily SSR anomalies in the MJO phases are shown in Fig. 8 (Phases 1, 2, 3, and 8 displaying non-significant pixels over the whole domain are not shown). Generally, the local SSR anomaly over Reunion and the surrounding ocean is consistent with the evolution of the global-scale MJO. Significant SSR anomalies are found over the study area but with low amplitude (~30 W m^{-2}) and barely over land, even in the phases with large anomalous convective activities (MJO phases 4, 5, 6, and 7).

As shown in Fig. 8, in phase 4 of the MJO, when the convection is enhanced in the tropical Indian Ocean, several pixels with significant negative SSR anomalies are found locally in the north of Reunion (mainly in the late afternoon, after 15:00). During phases 5 and 6, when the convective clusters move eastwards, and the tropical SWIO is covered by suppressed convective conditions, larger-scale and spatially coherent positive SSR anomalies are observed over land and nearby ocean (Fig. 8). During phase 5, anomalies are only significant during the afternoon, which correspond to the hours of largest cloud cover, on average, due to the diurnal cycle of convection in the tropics. These results are, therefore, consistent with a lower-than-normal convective activity in the region. By contrast, during phase 6, SSR anomalies are positive throughout the day, ranging from about 15 to 30 W m^{-2}, less than 5% of the multiyear seasonal mean in NDJF (Supplementary Figure S12). These results suggest that the MJO is likely to result in a statistically significant increase of SSR over Reunion and surrounding ocean during its dry/clear-sky phase, while its influence during the convectively active phase appears weaker and more uncertain. This is partly due to the fact that Reunion is located in the periphery of the core region of the MJO activity, where the amplitude of the MJO (OLR
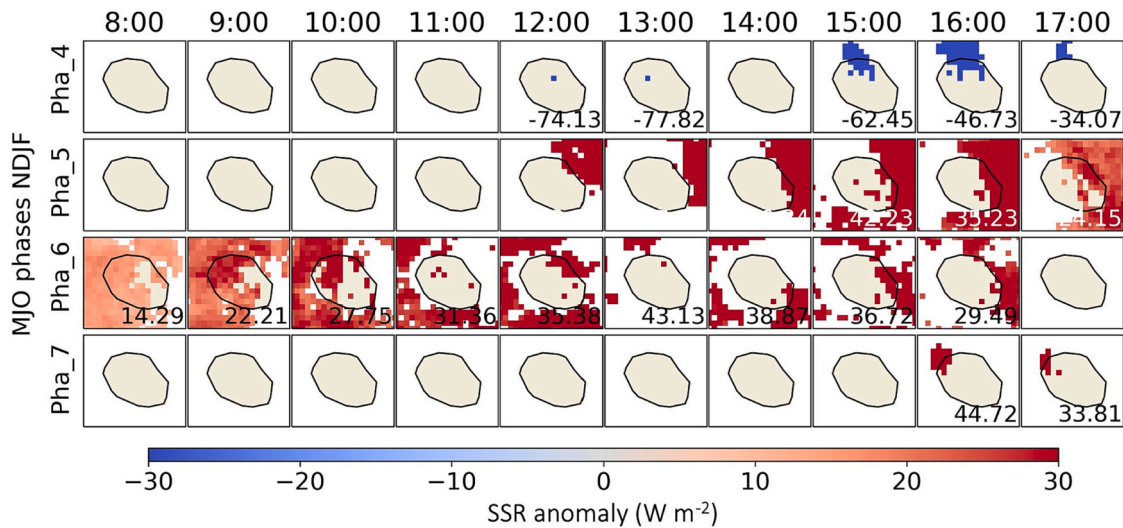
Fig. 8. The same as Fig. 6, but for the MJO phases (amplitude > 1) in NDJF. Phases 1, 2, 3, and 8 have no significant pixels over the entire domain and are therefore not shown.
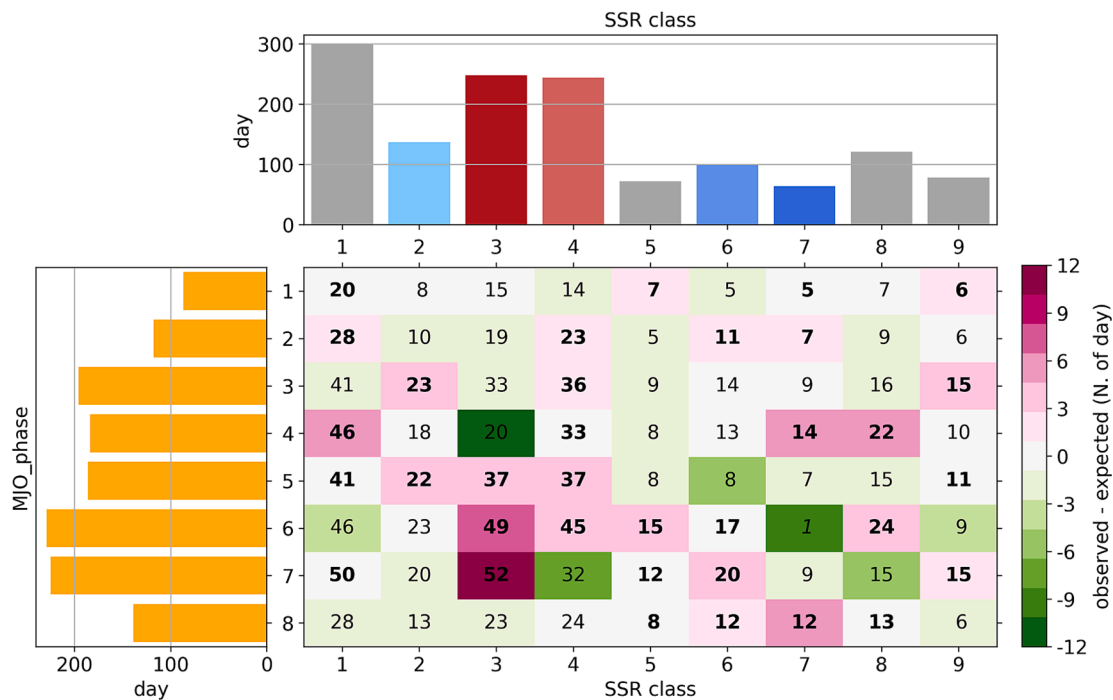

Fig. 9. The same as Fig. 7, but for the MJO phases (amplitude > 1) in NDJF.

anomalies) is less than 30 W m^{-2} (Supplementary Figure S5). Over tropical regions, such as the Maritime Continent, the diurnal cycle of tropical deep convection [74] and rainfall [75] are reported to be modified by the MJO, being enhanced/reduced (along with a stronger/weaker diurnal cycle) during the convectively active/suppressed phase of MJO.

The association between local SSR anomaly and the MJO can be inferred from a contingency map (Fig. 9). With significance, the MJO phase 6 is likely to induce a few negative SSR anomalies. In contrast, and consistent with the anomaly analysis (Fig. 8), no significance is found in the convectively suppressed phase of the MJO.

5. Interactions between the SSR drivers: TC, synoptic convective regimes, and the MJO

A nearby TC can strongly reduce SSR over Reunion, thus challenging the solar power output and reliability. In addition, the genesis and tracks of TCs in the SWIO have been reported as related to the regional TTTs (OLR regimes 5, 6, and 7; [76,77]) and the global MJO [78]. Furthermore, despite that TTTs have been reported to be statistically independent in terms of occurrence of the global-scale MJO activity [38,53], i.e., they are equally liable to occur during any phase of the MJO, the intensity of TTTs could be significantly, but weakly, modulated by the MJO phases [36], and thus affect local SSR in Reunion. Therefore, the possible interactions between TCs, synoptic convective regimes, and the MJO are investigated in this section to characterize better and separate their respective influence on local SSR in Reunion.

5.1. TCs in synoptic convective regimes

Firstly, a strong association of TCs with the synoptic convective activities is observed, for the first time, in the SWIO and in the area close to Reunion. Results are especially clear for OLR regime 1, which appear as the most favorable regime for TC occurrence. In the SWIO (see Fig. 10), up to 73.1% of the days in this regime are associated with TCs. This contrasts with the mean value in all regimes (about 44%, not shown) and with the other OLR regimes (less than 40%, except for regime 7, which has a value of about 50%). In addition, the geographical distribution of the TCs' tracks is, to some extent, coherent with the distribution of the enhanced convection (light blue contours in the same figure) in regime 1 in the northeast of Madagascar. This spatial coherence with TC locations can also be observed during occurrences of the central and eastern TTT systems (i.e., regimes 6–7) in the Mozambique Channel, being consistent with previous studies [77], while not in its early state (i.e., regime 5).

In the area close to Reunion (within 5°, where TC paths are shown in colored bold lines in Fig. 10), the occurrence of TCs in regimes 1 and 2, up to 16.7% and 15.6%, respectively, is much higher than the mean value of all the 7 regimes (6.1%, not shown) and the other regimes (less than 4.5%). Even though the ratio of nearby TC days and the TCs size (not shown) are similar in regimes 1 and 2, the associated SSR anomaly over Reunion are found to be quite different, the amplitude of negative SSR anomaly being much higher in regime 2 (Fig. 6). This is likely to be linked to the relative location of the TCs with respect to the island (see section 4.1). Within 5° of Reunion (the boldfaced-colored TC tracks in Fig. 10), the TCs are located more in the west in regime 2 (the median longitude is 53.4°E), where 79% of its TC-days are with negative SSR anomalies; in contrast, in regime 1, TCs are more in the east (the median

longitude is 56°E), where TCs are usually associated with less SSR attenuation or even positive SSR (54% of TC-days in regime 1 have negative SSR anomalies).

Secondly, the respective influence of nearby TCs and the OLR regimes is estimated by separating TC vs non-TC days that fall within each regime (Supplementary Figure S13, where regimes 3 to 7 with generally statistically insignificant pixels are not shown).

In the TC days, the OLR regime 2 has a higher amplitude of SSR anomaly (up to -230 W m^{-2}) compared with regime 1 (up to -180 W m^{-2}) with a similar number of TC days, which is likely due to the longitudinal dependence as discussed in section 4.1. In the non-TC days, negative SSR anomaly is found only in regime 2 with some positive pixels on the western coast of Reunion but no significant pixels in regime 1. Then the additivity reveals in regime 2: the strong negative influence of TCs in the TC days (up to -180 W m^{-2}) is reduced (up to -112 W m^{-2}) by combining with the influence of OLR regimes in the non-TC days (-96 W m^{-2}).

5.2. TCs in MJO phases

A significant association between the occurrence of TCs and the MJO has been observed in the SWIO and areas close (within 5°) to Reunion, as shown in Fig. 11. More TC days in the SWIO are found at a time when the convective center of the MJO is in the Eastern Indian Ocean (phases 2 and 3), and less TC days are found when the convective center is in the Western hemisphere and Africa (phases 1 and 8). This result agrees with previous works (e.g., [78]). In the area close to Reunion, more TC days are found in phase 2 and fewer in phase 7. However, these two phases, even though with significant associations of TCs, still produce a non-
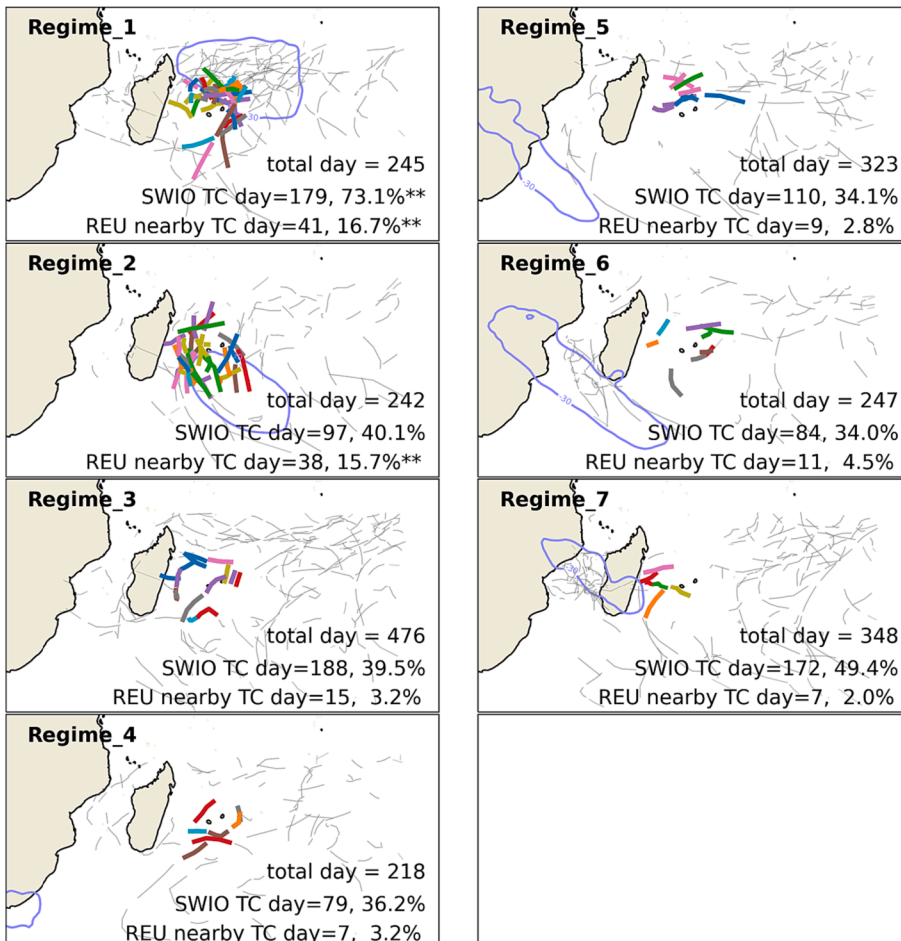

Fig. 10. Daily paths of TCs in the SWIO and within 5° of Reunion (21.1°S, 55.5°E, in boldfaced-colored lines) associated with each of the 7 OLR regimes. For Reunion nearby TCs, the path within a day is shown when at least one record (out of the 6-hourly data) in that day is within 5° of the island. The numbers of TCs in each regime over the SWIO and nearby Reunion are shown in each subplot with the percentages of the total number of days in that regime. In each regime, TC numbers significantly above average at the 95% level are indicated by **. The light blue contours depict the convective zones with a border of -30 W m^{-2} OLR anomaly. Note that the "total day" for each regime may be different from Fig. 6 since 1) in this figure, data after February 2016 is removed to match the availability of the TC dataset (up to April 2016) and 2) all the regimes in Fig. 6 are matched with SARAH-E data, which has missing values and values for the 29th of February have been removed as well. (For interpretation of the references to color in this figure legend, the reader is referred to the web version of this article.)
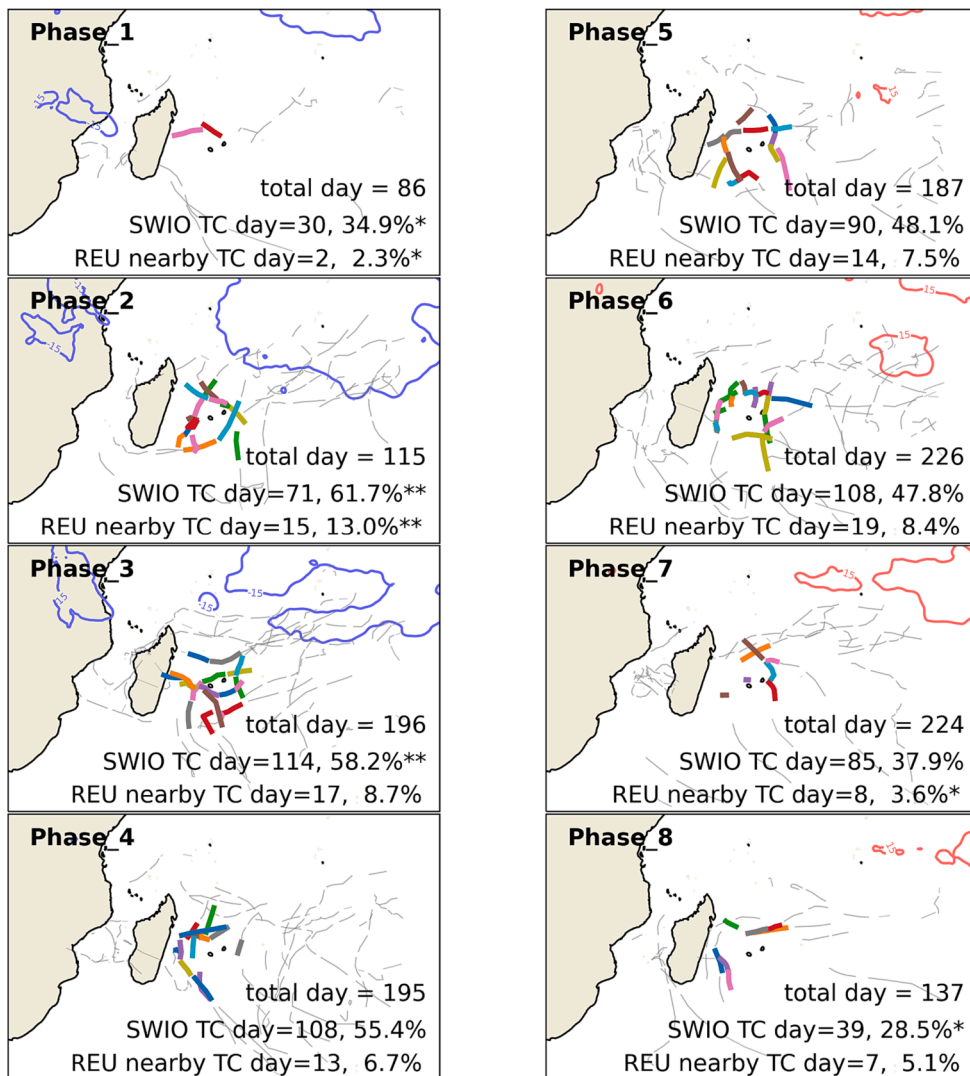
Fig. 11. Daily paths of TCs in the SWIO and within 5° of Reunion (21.1°S, 55.5°E, in boldfaced-colored lines) associated with each of the 8 high-amplitude (>1) MJO phases in NDJF season. For Reunion nearby TCs, the path within a day is shown when at least one record (out of the 6-hourly data) is within 5°. The numbers of TCs in each phase over the SWIO and nearby Reunion are shown in each subplot with the percentages of the total number of days in that phase. In each phase, numbers significantly above (below) average at the 95% level are indicated by ** (*). The light blue/red contours depict the convectively active / suppressed zones with a border of −15/15 W m^{-2} OLR anomaly. (For interpretation of the references to color in this figure legend, the reader is referred to the web version of this article.)

significant SSR anomaly over Reunion (section 4.3), which implies an internal variability of the sky conditions within MJO phases over Reunion caused probably by the large distance to the core of the MJO.

The respective influence of TCs and the MJO is estimated by investigating SSR anomaly in TC vs non-TC days in each MJO phase (Supplementary Figure S14 and Supplementary Figure S15, respectively). In the TC days, a statistically significant SSR anomaly is observed depending on the TCs' longitudinal position relative to the island (see Fig. 5). In phase 4, when the TCs are distributed in the west of Reunion (Supplementary Figure S14), strong negative anomalies are found up to −350 W m^{-2}. In contrast, in phase 7, when the TCs are located more in the east, some pixels with positive anomalies are found in the nearby ocean (even still insignificant over land). However, in the other phases (phases 1, 2, 5, 6, and 8), when TCs are equally distributed in the west and east, the associated SSR anomalies are generally insignificant (except for phase 3, which displays significant SSR anomaly but only in the morning). In the non-TC days, the significant SSR anomalies in the MJO phases are generally positive (phases 3, 5, 6, and 7; see Supplementary Figure S15). However, close to the northern coast of Reunion, several pixels with significant negative anomalies are found in phase 4.

When combining the influences by TCs (TC days) and the MJO phases (non-TC days), additivity is observed only when the nearly TCs are in the west of Reunion, and that is unrelated to the ratio of TC days. In the afternoon of phase 4, the small region of a limited number of negative pixels in the non-TC days is extended to a larger area (with

similar amplitude) by combining with the strong negative anomaly in TC days. In contrast, despite a statistically significant more TC occurrence in phase 2, the SSR anomaly is insignificant during neither the TC days (Supplementary Figure S14) nor the non-TC days (Supplementary Figure S15), and thus no additivity is found in phase 2. This is consistent with the fact that the nearby TCs are distributed in both the east and the west of the island (Fig. 11), and the eastern TCs may be associated with insignificant or positive SSR anomaly (Fig. 5).

5.3. Additivity between synoptic convective regimes and the MJO

This section establishes the potential interactions between the synoptic convective regimes (including TTTs) and the intraseasonal MJO, together with their possible covariation on SSR over Reunion. To quantify the additive effect on the local SSR variability over Reunion between intraseasonal and synoptic timescales, Fig. 12 shows the daily (8:00 to 17:00) mean SSR anomalies in the OLR regimes (1st row) associated with the MJO phases (amplitude > 1, 1st column) during NDJF, and in the form of their contingency matrix.

Fig. 12 first confirms that the occurrence of TTTs is not dependent on the MJO phases, thereby corroborating previous studies (e.g., Macron et al. [38], Pohl et al. [53]). The only significant value for TTTs regimes is found in OLR regime 6, showing that this regime is unlikely to happen during MJO phase 3. OLR regime 3, with a significantly positive daily mean SSR anomaly (mainly over the ocean), has higher mean values in
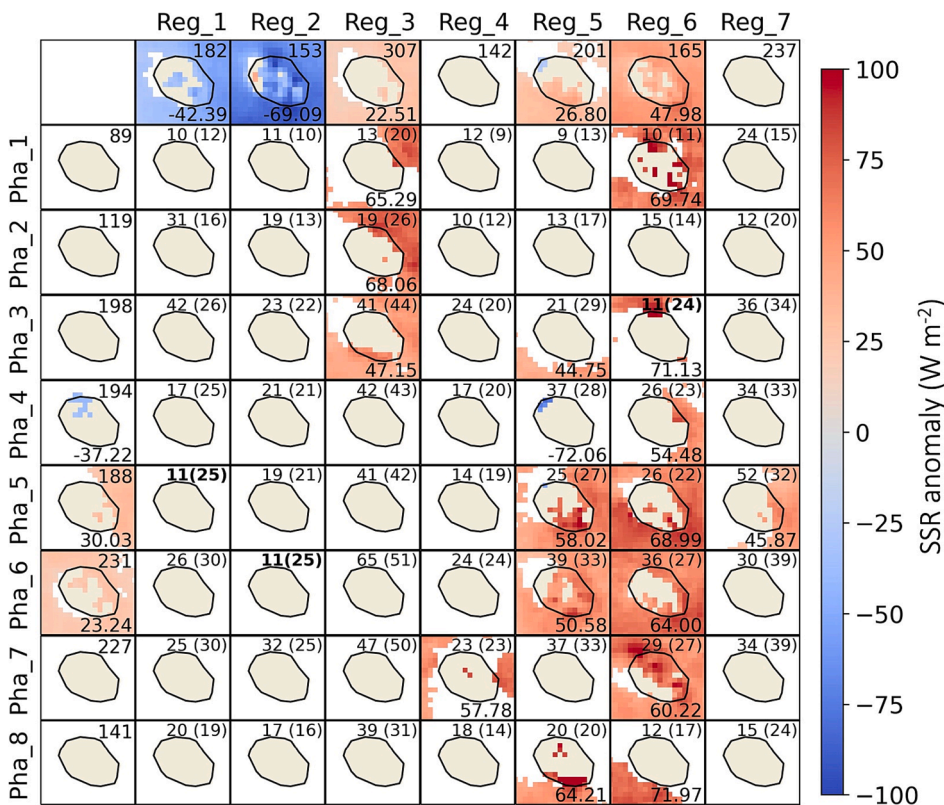
Fig. 12. Daily (8:00 – 17:00) mean SSR anomaly in NDJF of OLR regimes (1st row) and high amplitude (>1) MJO phases (1st column) and their contingency matrix. The number of days is on the upright of each plot, with expected values in brackets coming from an assumption of independent occurrence between OLR regimes and MJO phases. Bolds denote 95% significance according to Neu's test. Spatial mean values are on the bottom. Only the significant grid points of the SSR anomaly field are displayed according to Student's t-test with False Discovery Rate (FDR; [71]) correction at the 0.05 confidence level.

the days ascribed to MJO phases 1–3 when the convective center is in the tropical Indian Ocean, favoring a less convective atmosphere in the subtropical region. In regimes 5–6, the positive SSR anomalies are higher when associated with MJO phases 5 and 6, which indicates an additive effect on local SSR between the MJO and the TTTs, but with relatively few significant pixels over land. On the other hand, OLR regime 1 (2), with enhanced convection close to Reunion and significant negative SSR anomalies, shows significantly less coherence with MJO phase 5 (6), which is associated with suppressed convection and positive SSR anomaly in Reunion. However, the corresponding SSR anomaly is insignificant, indicating a high internal variability in MJO phases or OLR regimes. The latter could decrease the predictive skill of intraseasonal forecasts, mostly (but not only) based on MJO activity [79–81].

6. Conclusion and discussion

This work investigates the diurnal variability of SSR in Reunion and explores the links between this variability and its potential driving mechanisms. We analyze convective variability at synoptic and intra-seasonal timescales and scale interactions between them to assess the seamless predictability of SSR in the subtropical island of Reunion, characterized by complex topography.

Firstly, SSR diurnal variability is represented by an hourly-diurnal classification of satellite data from SARAH-E at ~5 km spatial resolution over Reunion, where the cluster transitions reflect a fluctuation of SSR at the synoptic timescale. This approach reveals several critical temporal and spatial characteristics of the diurnal SSR variability. Notably, a high probability (~55%) of uniform-sign SSR departures from the mean state throughout the day at the island-scale is found in the period from 1999-01-01 to 2016-12-31, either positive (~34%) or negative (~21%). SSR variability is also found to be larger on the windward side (at the east or southeast) of the island and during the warm season and smaller on the leeward side (at the west or northwest) and during the cold season. Such an SSR gradient between the east and the west could be necessary for the complementary strategy. Successive

negative events at the island scale, as represented by the transition of SSR clusters, typically last 1 or 2 days (the 75th percentile), which has to be fitted by the stabilizing efforts of solar power networks. Finally, a diurnal SSR cluster with large negative SSR anomalies (up to about −500 W m^{-2}) is primarily related to nearby TCs, which may pose a challenge for the solar power system due to the low level of SSR and the strong wind associated at synoptic timescale.

Secondly, an effort is made to understand how convective activities near Reunion, as drivers of its local-scale cloud cover and SSR, alter the diurnal SSR cycle in different ways, depending on their intensity, scale, and distance to the island. The key findings are as follows: (1) Nearby TCs, although at low occurrence, can enormously reduce the diurnal SSR, by up to 50% on average, depending on their distance and size; particularly, their influence on SSR is found to have a longitudinal dependence, which is observed for the first time, with significant negative SSR anomaly when TCs are in the west of Reunion and with less significant or even positive anomaly when in the east. (2) The modulation of SSR by synoptic convective regimes is relatively smaller, in the range from 5% to 13%. (3) At the intraseasonal timescale, the MJO is associated with a statistically significant increase in SSR over Reunion during its dry/clear-sky phase (less than 5%). In contrast, its influence during the convectively active phase appears weaker and more uncertain, mainly due to its larger scale.

Finally, potential interactions between these three SSR modulators are investigated. (1) A strong association of TCs with the synoptic convective regimes is observed, with high occurrence in the SWIO (regime 1) and in the area close to Reunion (regimes 1 and 2). The location of TCs is coherent with the convectively enhanced activities in the northeast of Madagascar (regime 1) and in the Mozambique channel (regimes 6 and 7, i.e., the central and eastern TTT systems), consistent with previous studies (e.g., Mavume et al., [77]). (2) With the intra-seasonal MJO, more TC days in the SWIO are recorded at a time when the convective center of the MJO is in the eastern Indian Ocean (phases 2 and 3), and less are found when the convective center is in the western hemisphere and Africa (phases 1 and 8), which corroborates previous

studies [78]. In the area close to Reunion, more TC days are associated with phase 2 of the MJO and fewer with phase 7, which could be another source of predictability of SSR in the subtropics, even not directly coupled with SSR. (3) Furthermore, the respective influence of TC and synoptic regimes and the MJO are separated. Additivity could be found only when the nearby TCs are in the west of Reunion in the OLR regime 2 and the MJO phase 4. (4) Finally, the additivity between the MJO and the synoptic regimes is not statistically significant, as reported by previous studies. In contrast, higher SSR anomalies are identified in the starting and the mature phases of a TTT before reaching their easternmost location, when co-occurring with phases 5 and 6 of the MJO with suppressed convection across the Indian Ocean and over tropical Africa.

These results provide quantitative insights into solar power system planning and management in many aspects, such as energy complementary strategy (in both space and time; [17,82]), PV output forecasting [23,83], and storage dimensioning technologies (e.g., Li-ion batteries, or hydrogen; [84–86]), to smooth out the expected imbalances between generation and demand at various temporal and spatial scales. The investigation conducted in this study has the potential to benefit not only Reunion but also the broader tropical and subtropical regions, owing to the extensive spatial coverage of these examined climate variability.

This study also confirmed that the TCs and the synoptic convective regimes are the primary modulators of SSR in the subtropical SWIO at the synoptic timescale. Additionally, the MJO, which is considered as a crucial predictability source in the tropics at the intraseasonal timescale [87], is likely to be another candidate that one could use to bridge the gap between daily weather and climate in the subtropics, as already proposed in other regions [88–90].

The present study underscores the appropriateness of the applied classification at high temporal (hourly-diurnal) and spatial (5 km) resolutions for representing the diurnal variability of SSR over a complex orography, as well as for examining its scale interactions with various modes of climate variability. This approach effectively captures the contrasted details in space, such as the difference between windward and leeward regions in diurnal SSR variability. Furthermore, the identified clusters can be utilized for transition analysis as temporal fluctuations and for investigating the links with driving mechanisms operating on larger timescales, including those of lower frequency, when datasets spanning longer periods are employed.

However, there are still open questions to complete the assessment of SSR variability locally and achieve fully decarbonized energy production. For instance, the SSR modulators assessed here for the first time have generally strong internal variability (e.g., Lin et al., [91]), and second-order modifications in their regional-scale anomaly patterns could yield major modifications locally over a tropical island like Reunion. Additional factors like sea surface temperature and land-sea contrasts could be considered in future work to complete our findings with more local-scale parameters that could also contribute to driving SST variability at fine scales. Furthermore, the potential SSR drivers at longer timescales, including both natural variability such as ENSO [92–94], but also anthropogenically-forced climate change [19,95–98], are crucial to consider in future research. This underscores the need for additional studies incorporating more SSR factors over a broader range of timescales and with improved spatial resolution to develop and enhance the seamless predictability of solar-related renewable energy applications.

CRediT authorship contribution statement

Chao Tang: Conceptualization, Methodology, Data curation, Investigation, Visualization, Writing – original draft, Writing – review & editing, Project administration. **Pauline Mialhe:** Methodology, Data curation, Investigation, Visualization. **Benjamin Pohl:** Conceptualization, Methodology, Investigation, Writing – review & editing. **Béatrice Morel:** Conceptualization, Writing – review & editing, Funding

acquisition, Resources, Project administration. **Martin Wild:** Investigation, Writing – review & editing. **Shunya Koseki:** Investigation, Writing – review & editing. **Babatunde Abiodun:** Investigation, Writing – review & editing. **Miloud Bessafi:** Funding acquisition. **Chris Lennard:** Investigation, Writing – review & editing. **Girish Kumar Beeharry:** Investigation, Writing – review & editing, Investigation, Writing – review & editing. **Roddy Lollchund:** Investigation, Writing – review & editing. **Tyagaraja S.M. Cunden:** Investigation, Writing – review & editing. **Swati Singh:** .

Declaration of Competing Interest

The authors declare that they have no known competing financial interests or personal relationships that could have appeared to influence the work reported in this paper.

Appendix A. Supplementary data

Supplementary data to this article can be found online at https://doi.org/10.1016/j.solener.2023.111856.

References

[1] IPCC, 2021. Climate Change 2021: The Physical Science Basis. Contribution of Working Group I to the Sixth Assessment Report of the Intergovernmental Panel on Climate Change. Cambridge University Press, Cambridge, United Kingdom and New York, NY, USA. In press.

[2] IEA, 2021a. Greenhouse Gas Emissions from Energy Data Explorer.

[3] Jäger-Waldau, A., 2021. Overview of the Global PV Industry☆, Reference Module in Earth Systems and Environmental Sciences. Elsevier.

[4] IEA, 2021. 2021b. World Energy. Outlook.

[5] Praene, J.P., Fakra, D.A.H., Benard, F., Ayagapin, L., Rachadi, M.N.M., 2021. Comoros's energy review for promoting renewable energy sources. Renewable Energy 169, 885–893.

[6] Praene, J.P., Radanielina, M.H., Rakotoson, V.R., Andriamamonjy, A.L., Sinama, F., Morau, D., Rakotondramiarana, H.T., 2017. Electricity generation from renewables in Madagascar: Opportunities and projections. Renewable and Sustainable Energy Reviews 76, 1066–1079.

[7] Utilities, M.o.E.a.P., 2019. RENEWABLE ENERGY ROADMAP 2030 FOR THE ELECTRICITY SECTOR.

[8] Praene, J.P., David, M., Sinama, F., Morau, D., Marc, O., 2012. Renewable energy: Progressing towards a net zero energy island, the case of Reunion Island. Renewable and Sustainable Energy Reviews 16 (1), 426–442.

[9] Selosse, S., Garabedian, S., Ricci, O., Maïzi, N., 2018. The renewable energy revolution of reunion island. Renewable and Sustainable Energy Reviews 89, 99–105.

[10] OER, 2019. BILAN ÉNERGÉTIQUE DE LA RÉUNION 2018 (ÉDITION 2019).

[11] Bénard-Sora, F., Praene, J.P., 2018. Sustainable urban planning for a successful energy transition on Reunion Island: From policy intentions to practical achievement. Utilities Policy 55, 1–13.

[12] Bessafi, M., Oree, V., Khoodaruth, A., Jumaux, G., Bonnardot, F., Jeanty, P., Delsaut, M., Chabriat, J.-P., Dauhoo, M.Z., 2018. Downscaling solar irradiance using DEM-based model in young volcanic islands with rugged topography. Renewable Energy 126, 584–593.

[13] Diagne, M., David, M., Lauret, P., Boland, J., Schmutz, N., 2013. Review of solar irradiance forecasting methods and a proposition for small-scale insular grids. Renewable and Sustainable Energy Reviews 27, 65–76.

[14] André, M., Perez, R., Soubdhan, T., Schlemmer, J., Calif, R., Monjoly, S., 2019. Preliminary assessment of two spatio-temporal forecasting technics for hourly satellite-derived irradiance in a complex meteorological context. Solar Energy 177, 703–712.

[15] Fouilloy, A., Voyant, C., Notton, G., Motte, F., Paoli, C., Nivet, M.-L., Guillot, E., Duchaud, J.-L., 2018. Solar irradiation prediction with machine learning: Forecasting models selection method depending on weather variability. Energy 165, 620–629.

[16] Mejia, J.F., Giordano, M., Wilcox, E., 2018. Conditional summertime day-ahead solar irradiance forecast. Solar Energy 163, 610–622.

[17] Jurasz, J., Canales, F.A., Kies, A., Guezgouz, M., Beluco, A., 2020. A review on the complementarity of renewable energy sources: Concept, metrics, application and future research directions. Solar Energy 195, 703–724.

[18] Liu, L., Wang, Z., Wang, Y., Wang, J., Chang, R., He, G., Tang, W., Gao, Z., Li, J., Liu, C., Zhao, L., Qin, D., Li, S., 2020. Optimizing wind/solar combinations at finer scales to mitigate renewable energy variability in China. Renewable and Sustainable Energy Reviews 132, 110151.

[19] Wild, M., Folini, D., Henschel, F., Fischer, N., Müller, B., 2015. Projections of long-term changes in solar radiation based on CMIP5 climate models and their influence on energy yields of photovoltaic systems. Solar Energy 116, 12–24.

[20] Yin, J., Molini, A., Porporato, A., 2020. Impacts of solar intermittency on future photovoltaic reliability. Nature Communications 11 (1), 4781.

[21] Perez, R., David, M., Hoff, T.E., Jamaly, M., Kivalov, S., Kleissl, J., Lauret, P., Perez, M., 2016. Spatial and temporal variability of solar energy. Now Publishers 1 (1), 1–44.

[22] Badosa, J., Haeffelin, M., Chepfer, H., 2013. Scales of spatial and temporal variation of solar irradiance on Reunion tropical island. Solar Energy 88, 42–56.

[23] Badosa, J., Haeffelin, M., Kalecinski, N., Bonnardot, F., Jumaux, G., 2015. Reliability of day-ahead solar irradiance forecasts on Reunion Island depending on synoptic wind and humidity conditions. Solar Energy 115, 306–321.

[24] Jumaux, G., Quetelard, H., Roy, D., 2011. Atlas climatique de la Réunion. Météo-France, Direction interrégionale de la Réunion.

[25] Li, P., Li, Q., 2022. Intraseasonal and synoptic climate variability of surface solar radiation over South-West Indian Ocean: Regional climate modelling. International Journal of Climatology 42 (8), 4405–4423.

[26] Mialhe, P., Pohl, B., Morel, B., Trentmann, J., Jumaux, G., Bonnardot, F., Bessafi, M., Chabriat, J.-P., 2020. On the determination of coherent solar climates over a tropical island with a complex topography. Solar Energy 206, 508–521.

[27] Leroux, M.-D., Meister, J., Mekies, D., Dorla, A.-L., Caroff, P., 2018. A Climatology of Southwest Indian Ocean Tropical Systems: Their Number, Tracks, Impacts, Sizes, Empirical Maximum Potential Intensity, and Intensity Changes. Journal of Applied Meteorology and Climatology 57 (4), 1021–1041.

[28] Robinson, G., Watson, K., Walker, A., Desai, J., Van Geet, O., Elsworth, J., Gunda, T., 2021. Weather impacts on solar PV operations summary of the current body of knowledge and implications for further investigation. United States, p. Medium: ED; Size: 98 p.

[29] Fauchereau, N., Pohl, B., Reason, C., Rouault, M., Richard, Y., 2009. Recurrent daily OLR patterns in the Southern Africa/Southwest Indian Ocean region, implications for South African rainfall and teleconnections. Climate Dynamics 32 (4), 575–591.

[30] Hart, N.C.G., Reason, C.J.C., Fauchereau, N., 2010. Tropical-Extratropical Interactions over Southern Africa: Three Cases of Heavy Summer Season Rainfall. Monthly Weather Review 138 (7), 2608–2623.

[31] Macron, C., Pohl, B., Richard, Y., Bessafi, M., 2014. How do Tropical Temperate Troughs Form and Develop over Southern Africa? Journal of Climate 27 (4), 1633–1647.

[32] Pohl, B., Dieppois, B., Crétat, J., Lawler, D., Rouault, M., 2018. From synoptic to interdecadal variability in Southern African rainfall: toward a unified view across time scales. Journal of Climate 31 (15), 5845–5872.

[33] Ratna, S.B., Behera, S., Ratnam, J.V., Takahashi, K., Yamagata, T., 2013. An index for tropical temperate troughs over southern Africa. Climate dynamics 41 (2), 421–441.

[34] Todd, M.C., Washington, R., Palmer, P.I., 2004. Water vapour transport associated with tropical–temperate trough systems over southern Africa and the southwest Indian Ocean. International Journal of Climatology 24 (5), 555–568.

[35] Vigaud, N., Pohl, B., Crétat, J., 2012. Tropical-temperate interactions over Southern Africa simulated by a regional climate model. Climate Dynamics 39 (12), 2895–2916.

[36] Hart, N.C.G., Reason, C.J.C., Fauchereau, N., 2013. Cloud bands over southern Africa: seasonality, contribution to rainfall variability and modulation by the MJO. Climate Dynamics 41 (5), 1199–1212.

[37] Todd, M., Washington, R., 1999. Circulation anomalies associated with tropical-temperate troughs in southern Africa and the south west Indian Ocean. Climate dynamics 15 (12), 937–951.

[38] Macron, C., Richard, Y., Garot, T., Bessafi, M., Pohl, B., Ratiarison, A., Razafindrabe, A., 2016. Intraseasonal Rainfall Variability over Madagascar. Monthly Weather Review 144 (5), 1877–1885.

[39] Madden, R.A., Julian, P.R., 1971. Detection of a 40–50 Day Oscillation in the Zonal Wind in the Tropical Pacific. Journal of Atmospheric Sciences 28 (5), 702–708.

[40] Madden, R.A., Julian, P.R., 1972. Description of Global-Scale Circulation Cells in the Tropics with a 40–50 Day Period. Journal of Atmospheric Sciences 29 (6), 1109–1123.

[41] Madden, R.A., Julian, P.R., 1994. Observations of the 40–50-Day Tropical Oscillation—A Review. Monthly Weather Review 122 (5), 814–837.

[42] Zhang, C., 2005. Madden-Julian Oscillation. Reviews of Geophysics 43 (2).

[43] Zhang, C., 2013. Madden–Julian Oscillation: Bridging Weather and Climate. Bulletin of the American Meteorological Society 94 (12), 1849–1870.

[44] Pohl, B., Matthews, A.J., 2007. Observed Changes in the Lifetime and Amplitude of the Madden–Julian Oscillation Associated with Interannual ENSO Sea Surface Temperature Anomalies. Journal of Climate 20 (11), 2659–2674.

[45] Wheeler, M.C., Hendon, H.H., 2004. An All-Season Real-Time Multivariate MJO Index: Development of an Index for Monitoring and Prediction. Monthly Weather Review 132 (8), 1917–1932.

[46] Moncrieff, M.W., Waliser, D.E., Miller, M.J., Shapiro, M.A., Asrar, G.R., Caughey, J., 2012. Multiscale Convective Organization and the YOTC Virtual Global Field Campaign. Bulletin of the American Meteorological Society 93 (8), 1171–1187.

[47] Camberlin, P., Gitau, W., Kiladis, G., Bosire, E., Pohl, B., 2019. Intraseasonal to Interannual Modulation of Diurnal Precipitation Distribution Over Eastern Africa. Journal of Geophysical Research: Atmospheres 124 (22), 11863–11886.

[48] Pohl, B., Camberlin, P., 2006. Influence of the Madden–Julian Oscillation on East African rainfall. I: Intraseasonal variability and regional dependency. Quarterly Journal of the Royal Meteorological Society 132 (621), 2521–2539.

[49] Xu, W., Rutledge, S.A., 2014. Convective Characteristics of the Madden–Julian Oscillation over the Central Indian Ocean Observed by Shipborne Radar during DYNAMO. Journal of the Atmospheric Sciences 71 (8), 2859–2877.

[50] Meyers, G., McIntosh, P., Pigot, L., Pook, M., 2007. The Years of El Niño, La Niña, and Interactions with the Tropical Indian Ocean. Journal of Climate 20 (13), 2872–2880.

[51] Saji, N.H., Goswami, B.N., Vinayachandran, P.N., Yamagata, T., 1999. A dipole mode in the tropical Indian Ocean. Nature 401 (6751), 360–363.

[52] Behera, S.K., Yamagata, T., 2001. Subtropical SST dipole events in the southern Indian Ocean. Geophysical Research Letters 28 (2), 327–330.

[53] Pohl, B., Fauchereau, N., Richard, Y., Rouault, M., Reason, C.J.C., 2009. Interactions between synoptic, intraseasonal and interannual convective variability over Southern Africa. Climate Dynamics 33 (7-8), 1033–1050.

[54] Lesouëf, D., Gheusi, F., Delmas, R., Escobar, J., 2011. Numerical simulations of local circulations and pollution transport over Reunion Island. Ann. Geophys. 29 (1), 53–69.

[55] ASTER, 2019. ASTER Global Digital Elevation Model V003.

[56] Réchou, A., Flores, O., Jumaux, G., Duflot, V., Bousquet, O., Pouppeville, C., Bonnardot, F., 2019. Spatio-temporal variability of rainfall in a high tropical island: Patterns and large-scale drivers in Réunion Island. Quarterly Journal of the Royal Meteorological Society 145 (720), 893–909.

[57] Morel, B., Pohl, B., Richard, Y., Bois, B., Bessafi, M., 2014. Regionalizing Rainfall at Very High Resolution over La Réunion Island Using a Regional Climate Model. Monthly Weather Review 142 (8), 2665–2686.

[58] Pohl, B., Morel, B., Barthe, C., Bousquet, O., 2016. Regionalizing Rainfall at Very High Resolution over La Réunion Island: A Case Study for Tropical Cyclone Ando. Monthly Weather Review 144 (11), 4081–4099.

[59] Amillo, A.G., Huld, T., Müller, R., 2014. A New Database of Global and Direct Solar Radiation Using the Eastern Meteosat Satellite. Models and Validation. Remote Sensing 6 (9), 8165–8189.

[60] Huld, T., Müller, R., Gracia-Amillo, A., Pfeifroth, U., Trentmann, J., 2017. Surface Solar Radiation Data Set-Heliosat, Meteosat-East (SARAH-E). Satell. Appl. Facil. Clim, Monit.

[61] Riihelä, A., Kallio, V., Devraj, S., Sharma, A., Lindfors, A.V., 2018. Validation of the SARAH-E Satellite-Based Surface Solar Radiation Estimates over India. Remote Sensing 10 (3), 392.

[62] Wang, Y., Trentmann, J., Yuan, W., Wild, M., 2018. Validation of CM SAF CLARA-A2 and SARAH-E Surface Solar Radiation Datasets over China. Remote Sensing 10 (12), 1977.

[63] Ward, J.H., 1963. Hierarchical Grouping to Optimize an Objective Function. Journal of the American Statistical Association 58 (301), 236–244.

[64] Hersbach, H., Bell, B., Berrisford, P., Hirahara, S., Horányi, A., Muñoz-Sabater, J., Nicolas, J., Peubey, C., Radu, R., Schepers, D., Simmons, A., Soci, C., Abdalla, S., Abellan, X., Balsamo, G., Bechtold, P., Biavati, G., Bidlot, J., Bonavita, M., Chiara, G., Dahlgren, P., Dee, D., Diamantakis, M., Dragani, R., Flemming, J., Forbes, R., Fuentes, M., Geer, A., Haimberger, L., Healy, S., Hogan, R.J., Hólm, E., Janisková, M., Keeley, S., Laloyaux, P., Lopez, P., Lupu, C., Radnoti, G., Rosnay, P., Rozum, I., Vamborg, F., Villaume, S., Thépaut, J.-N., 2020. The ERA5 global reanalysis. Quarterly Journal of the Royal Meteorological Society 146 (730), 1999–2049.

[65] Cheng, X., Wallace, J.M., 1993. Cluster Analysis of the Northern Hemisphere Wintertime 500-hPa Height Field: Spatial Patterns. Journal of Atmospheric Sciences 50 (16), 2674–2696.

[66] Michelangeli, P.-A., Vautard, R., Legras, B., 1995. Weather Regimes: Recurrence and Quasi Stationarity. Journal of Atmospheric Sciences 52 (8), 1237–1256.

[67] Pohl, B., Lorrey, A., Sturman, A., Quénol, H., Renwick, J., Fauchereau, N., Pergaud, J., 2021. "Beyond Weather Regimes": Descriptors Monitoring Atmospheric Centers of Action—A Case Study for Aotearoa New Zealand. Journal of Climate 34 (20), 8341–8360.

[68] Pohl, B., Saucède, T., Favier, V., Pergaud, J., Verfaillie, D., Féral, J.-P., Krasniqi, Y., Richard, Y., 2021. Recent Climate Variability around the Kerguelen Islands (Southern Ocean) Seen through Weather Regimes. Journal of Applied Meteorology and Climatology 60 (5), 711–731.

[69] Barbary, D., Leroux, M.-D., Bousquet, O., 2019. The orographic effect of Reunion Island on tropical cyclone track and intensity. Atmospheric Science Letters 20 (2), e882.

[70] Landsea, C.W., Cangialosi, J.P., 2018. Have We Reached the Limits of Predictability for Tropical Cyclone Track Forecasting? Bulletin of the American Meteorological Society 99 (11), 2237–2243.

[71] Benjamini, Y., 2010. Discovering the false discovery rate. Journal of the Royal Statistical Society: Series B (Statistical Methodology) 72(4), 405-416.

[72] Neu, C.W., Byers, C.R., Peek, J.M., 1974. A technique for analysis of utilization-availability data. The Journal of Wildlife Management 38 (3), 541.

[73] Pohl, B., Camberlin, P., 2014. A typology for intraseasonal oscillations. International Journal of Climatology 34 (2), 430–445.

[74] Tian, B., Waliser, D.E., Fetzer, E.J., 2006. Modulation of the diurnal cycle of tropical deep convective clouds by the MJO. Geophysical Research Letters 33 (20).

[75] Oh, J.-H., Kim, K.-Y., Lim, G.-H., 2012. Impact of MJO on the diurnal cycle of rainfall over the western Maritime Continent in the austral summer. Climate Dynamics 38 (5), 1167–1180.

[76] Ash, K.D., Matyas, C.J., 2012. The influences of ENSO and the subtropical Indian Ocean Dipole on tropical cyclone trajectories in the southwestern Indian Ocean. International Journal of Climatology 32 (1), 41–56.

[77] Mavume, A.F., Rydberg, L., Rouault, M., Lutjeharms, J.R., 2009. Climatology and landfall of tropical cyclones in the south-west Indian Ocean. Western Indian Ocean Journal of Marine Science 8 (1).

[78] Bessafi, M., Wheeler, M.C., 2006. Modulation of South Indian Ocean Tropical Cyclones by the Madden–Julian Oscillation and Convectively Coupled Equatorial Waves. Monthly Weather Review 134 (2), 638–656.

[79] Graham, R.M., Browell, J., Bertram, D., White, C.J., 2022. The application of sub-seasonal to seasonal (S2S) predictions for hydropower forecasting. Meteorological Applications 29 (1), e2047.

[80] Gudoshava, M., Wanzala, M., Thompson, E., Mwesigwa, J., Endris, H.S., Segele, Z., Hirons, L., Kipkogei, O., Mumbua, C., Njoka, W., Baraibar, M., de Andrade, F., Woolnough, S., Atheru, Z., Artan, G., 2022. Application of real time S2S forecasts over Eastern Africa in the co-production of climate services. Climate Services 27, 100319.

[81] Vitart, F., Robertson, A.W., 2018. The sub-seasonal to seasonal prediction project (S2S) and the prediction of extreme events. npj Climate and Atmospheric. Science 1 (1), 3.

[82] Weschenfelder, F., de Novaes Pires Leite, G., Araújo da Costa, A.C., de Castro Vilela, O., Ribeiro, C.M., Villa Ochoa, A.A., Araújo, A.M., 2020. A review on the complementarity between grid-connected solar and wind power systems. Journal of Cleaner Production 257, 120617.

[83] Mellit, A., Massi Pavan, A., Ogliari, E., Leva, S., Lughi, V., 2020. Advanced Methods for Photovoltaic Output Power Forecasting: A Review. Applied Sciences 10 (2), 487.

[84] Agbossou, K., Chahine, R., Hamelin, J., Laurencelle, F., Anouar, A., St-Arnaud, J. M., Bose, T.K., 2001. Renewable energy systems based on hydrogen for remote applications. Journal of Power Sources 96 (1), 168–172.

[85] Olabi, A.G., 2017. Renewable energy and energy storage systems. Energy 136, 1–6.

[86] Yang, Y., Bremner, S., Menictas, C., Kay, M., 2018. Battery energy storage system size determination in renewable energy systems: A review. Renewable and Sustainable Energy Reviews 91, 109–125.

[87] Waliser, D., Weickmann, K., Dole, R., Schubert, S., Alves, O., Jones, C., Newman, M., Pan, H.-L., Roubicek, A., Saha, S., Smith, C., Van den Dool, H., Vitart, F., Wheeler, M., Whitaker, J., 2006. The Experimental MJO Prediction Project. Bull. Amer. Meteor. Soc. 87 (4), 425–431.

[88] Jia, X., Chen, L., Ren, F., Li, C., 2011. Impacts of the MJO on winter rainfall and circulation in China. Advances in Atmospheric Sciences 28 (3), 521–533.

[89] Juliá, C., Rahn, D.A., Rutllant, J.A., 2012. Assessing the Influence of the MJO on Strong Precipitation Events in Subtropical, Semi-Arid North-Central Chile (30°S). Journal of Climate 25 (20), 7003–7013.

[90] Kim, B.-M., Lim, G.-H., Kim, K.-Y., 2006. A new look at the midlatitude–MJO teleconnection in the northern hemisphere winter. Quarterly Journal of the Royal Meteorological Society 132 (615), 485–503.

[91] Lin, H., Brunet, G., Yu, B., 2015. Interannual variability of the Madden-Julian Oscillation and its impact on the North Atlantic Oscillation in the boreal winter. Geophysical Research Letters 42 (13), 5571–5576.

[92] Mohammadi, K., Goudarzi, N., 2018. Study of inter-correlations of solar radiation, wind speed and precipitation under the influence of El Niño Southern Oscillation (ENSO) in California. Renewable Energy 120, 190–200.

[93] Murari, T.B., Filho, A.S.N., Moret, M.A., Pitombo, S., Santos, A.A.B., 2020. Self-Affine Analysis of ENSO in Solar Radiation. Energies 13 (18), 4816.

[94] Pinker, R.T., Grodsky, S.A., Zhang, B., Busalacchi, A., Chen, W., 2017. ENSO impact on surface radiative fluxes as observed from space. Journal of Geophysical Research: Oceans 122 (10), 7880–7896.

[95] Creutzig, F., Agoston, P., Goldschmidt, J.C., Luderer, G., Nemet, G., Pietzcker, R.C., 2017. The underestimated potential of solar energy to mitigate climate change. Nature Energy 2 (9), 17140.

[96] Leroux, M.D., Bonnardot, F., Kotomangazafy, S., Veerabadren, P., Oikil Ridhoine, A., Somot, S., Alias, A., Chauvin, F., 2021. Regional climate projections and associated climate services in the southwest Indian ocean basin, EGU General Assembly Conference Abstracts. pp. EGU21-7029.

[97] Patt, A., Pfenninger, S., Lilliestam, J., 2013. Vulnerability of solar energy infrastructure and output to climate change. Climatic Change 121 (1), 93–102.

[98] Tang, C., Morel, B., Wild, M., Pohl, B., Abiodun, B., Bessafi, M., Lennard, C., 2019. Numerical simulation of surface solar radiation over Southern Africa. Part 2: Projections of regional and global climate models. Climate Dynamics.